# Characteristics of Deep Convection from Nadir-Viewing High-Altitude Airborne Doppler Radar

**Gerald M. Heymsfield[1], Lin Tian[2], Andrew J. Heymsfield[3] , Lihua Li[1], and Stephen Guimond[4]**

[1]NASA/ Goddard Space Flight Center, Greenbelt, Maryland, USA
[2]University of Maryland, UMBC/GEST, Baltimore County, Maryland, USA
[3]National Center for Atmospheric Research, Boulder, Colorado, USA
[4] Department of Meteorology, Florida State University, Tallahassee, Florida, USA

Submitted to *Journal of the Atmospheric Science*
*March, 2009*

---

*Corresponding author:* Gerald M. Heymsfield, Goddard Space Flight Center, Code 613.1, Greenbelt, MD 20771; gerald.heymsfield@nasa.gov

**Abstract**

This paper presents observations of deep convection characteristics in the tropics and subtropics that have been classified into four categories: tropical cyclone, oceanic, land, and sea breeze. Vertical velocities in the convection were derived from Doppler radar measurements collected during several NASA field experiments from the nadir-viewing high-altitude ER-2 Doppler Radar (EDOP). Emphasis is placed on the vertical structure of the convection from the surface to cloud top (sometimes reaching 18 km altitude). This unique look at convection is not possible from other approaches such as ground-based or lower altitude airborne scanning radars. The vertical motions from the radar measurements are derived using new relationships between radar reflectivity and hydrometeor fallspeed. Various convective properties, such as the peak updraft and downdraft velocities and their corresponding altitude, heights of reflectivity levels, and widths of reflectivity cores, are estimated.

The most significant findings are the following: 1) strong updrafts mostly exceed 15 m $s^{-1}$ with a few exceeding 30 m $s^{-1}$ are found in all the deep convection cases, whether over land or ocean 2) peak updrafts were almost always above the 10 km level and in the case of tropical cyclones, closer to the 12 km level; and 3) land-based and sea breeze convection had higher reflectivities and wider convective cores than oceanic and tropical cyclone convection. The results are discussed in terms of dynamical and microphysical implications for numerical models and future remote sensors.

## 1. Introduction

Measurements of updraft characteristics are important for understanding fundamental kinematic and microphysical processes in deep convection. These measurements are often difficult to obtain from *in situ* observations due to the transient nature of updrafts and the safety concerns arising from aircraft penetrating convective cores. Consequently, there have been relatively few comparisons between numerically simulated and measured vertical motions through the full depth of deep convective updrafts to evaluate model accuracy (e.g. Lang et al. 2007). Emphasis in recent years on global estimates of tropical latent heating from radar and microwave radiometric measurements on the Tropical Rain Measuring Mission (TRMM; Simpson et al. 1996) requires improved knowledge of the vertical motions in precipitation regions since this quantity is not measured. Deep convection distributes heat and moisture in the vertical and is therefore of crucial importance in understanding the dynamics of tropical (and subtropical) regions.

There have been numerous studies of tropical and subtropical convection using aircraft *in situ* measurements of updrafts (e.g., LeMone and Zipser, 1980; Jorgensen and Lemone, 1989, Anderson et al., 2005). In hurricanes, for example, Jorgensen et al. (1985) found that the strongest 10% of updrafts and downdrafts in hurricanes had averages of 4.2 and 2.6 m $s^{-1}$, respectively. Previous studies of tropical oceanic convection show weak vertical velocities partly because the measurements were derived from lower altitude aircraft as well as systematic uncertainties arising from aircraft sampling. Anderson et al. (2005) examined updrafts in tropical convective storms using the measurements from a Citation jet aircraft to examine similarities between tropical oceanic and land cases from TRMM Large Scale Biosphere-Atmosphere (LBA) and the Kwajalein Experiment (KWAJEX). Unlike earlier studies that used flight level data, Black et al. (1996) used radial velocities from the National Oceanic and Atmospheric Administration NOAA WP-3D tail Doppler radar and reported supercell-like structure in Hurricane Emily (1987) with updrafts and downdrafts as strong as 24 and 19 m $s^{-1}$, respectively. They found that in the eyewall region, 5% of the vertical motions were > 5 m $s^{-1}$. There have been numerous ground-based multiple Doppler measurements of convection in the tropics and subtropics but fewer measurements over the oceans that have been derived from either in situ or airborne Doppler radar measurements. One would expect that the geographic location and meteorological phenomenon would greatly affect the updraft characteristics in deep convection. The convective storm environment deduced from soundings (e.g. CAPE, vertical shear) and low level forcing, can be drastically different leading to different attributes of convection.

Recent attention has focused on hot towers and vortical hot towers in tropical cyclones since they may have important implications for tropical cyclone intensification as shown by both theoretical (e.g., Montgomery et al. 2006) and observational (e.g., Simpson et al. 1998; Heymsfield et al. 2001, 2006) studies. Observations of hot towers from high resolution radar measurements (Simpson et al. 1998; Heymsfield et al. 2001; Heymsfield et al. 2006, Halverson et al. 2007, Houze et al. 2009) have shown that hot towers can be very intense extending to 17 or 18 km altitude with strong updrafts and high reflectivities aloft. In light of this recent work, an important question is: How do tropical cyclone hot towers compare with more ordinary intense convection? Improved understanding of hot towers and their role in hurricane intensification will require finer spatial and temporal observational knowledge of their kinematic and microphysical characteristics. The first order measurement of intense convection that is linked to these processes is the strength of the vertical motions, which is the emphasis of this paper.

Satellite measurements have been used to define general characteristics of tropical convection. Zipser et al. (2006) studied the most intense thunderstorms within the coverage of TRMM (35S to 35N latitude) focusing on four parameters of intense convective storms: three-dimensional radar reflectivity, lightning, passive microwave, and visible/infrared channels. The TRMM satellite does not have Doppler radar measurements so it cannot directly provide information on vertical motions. Zipser et al. (2006) define "intense" storms using the available TRMM measurements as proxies for convective intensity. Common definitions of intense storms derived primarily from ground-based radar measurements include updrafts > 25 m $s^{-1}$, hail > 1.9 cm in diameter, or the presence of a tornado (Zipser et al. 2006). The TRMM proxies used by Zipser et al. (2006), Cecil et al. (2005), Nesbitt et al. (2000), and others equate increased storm intensity with: 1) increasing height of the 40 dBZ echo above 10 km altitude, 2) decreasing brightness temperatures at 37 and 85 GHz and 3) greater lightning flash rates in the precipitation feature. The common property governing all of these proxies is the strength of the vertical motions and thus, there is a need to better understand the relationship between microphysical and kinematic processes in deep convection. TRMM and the future Global Precipitation Mission (GPM; Hou et al. 2009) uses radar reflectivity and radiometer measurements along with cloud models to infer latent heating. Knowledge of vertical winds can be extremely useful in providing higher accuracy computations of latent heat either through model improvement or direct use of the observations, such as high-altitude airborne Doppler radar measurements.

Deep convection plays a key role in transport and mixing in the tropical tropopause layer (14 – 18 km altitude; e.g. Sherwood and Dessler 2000). Extensive upper troposphere cirrus layers in the tropics are often generated by ice mass from deep convective updrafts. The amount of cirrus produced is a complex function of vertical motions and microphysics.  Liu and Zipser (2005) suggested that the more intense the convection, the more likely the radar echo top is to the IR top derived from infrared radiation indicating a larger potential for mass exchange in the tropical tropopause layer.  It is well known that there is a general relationship between updraft strength and the amount of cloud top overshoot into the tropopause (e.g., Heymsfield 1991, Adler and Mack 1986).  Adler and Mack (1986), through modeling of mid-latitude severe storms, showed that overshooting cloud parcels that are strongly negatively buoyant will mix with the lower stratospheric environment and eventually subside.  Deep convective updraft properties in this higher altitude region have not been measured adequately due to the lack of observations.  In addition, downdrafts at all altitudes (particularly upper levels) have not been measured extensively and their documentation in the literature is sparse.  Heymsfield et al. (1985) found the presence of strong (> 10 m $s^{-1}$) upper level downdrafts from ground-based Doppler analyses that occurred as a result of convergence produced by two adjacent storm outflows.  Sun et al. (1994) suggested that upper level downdrafts can be produced by vertical pressure gradient forces.  Buoyancy driven downdrafts are also possible.  Early theoretical studies on convective updrafts derived from the vertical equation of motion and the thermodynamic equation in which parcels undergo adiabatic ascent and buoyancy, entrainment, and hydrometeor drag are important factors (e.g., Stommel 1947, Simpson and Wiggert 1969).  These models provide insights on the basic physics of convection but are often too simplistic to account for all the complex processes.  Lucas et al. (1994) theorized that updraft width and strength are correlated because mixing and entrainment will, in general, reduce the buoyancy of air parcels.  There is still debate over the amount of entrainment in tropical convection and whether tropical oceanic convection is dilute or undiluted (e.g., Zipser 2003).  These observations provide motivation to learn more about updraft characteristics in tropical convection and their variations with height.

In this paper, we utilize high-resolution airborne observations from the downward looking NASA ER-2 Doppler Radar (EDOP) to examine vertical motion characteristics during multiple field campaigns dealing with tropical and subtropical deep convection, including hurricanes. Previous observations have stimulated our interest in understanding, for example, if the structure of hurricane hot towers is different from ordinary deep tropical convection.

Section 2 will describe the cases sampled and the analysis methodology for both estimation of vertical velocities and for deriving statistical information from the data. Section 3 presents characteristics of the updrafts to learn more about the regional variation of reflectivity heights and vertical velocity as well as the relationship between peak updraft speeds and reflectivity contour levels. These observational details are important as they have implications for understanding convective dynamics including mass fluxes and latent heating. The statistics presented in section 3 will be compared with previous satellite-based and aircraft-based convection measurements (e.g., Black et al. 1996). Another important aspect of the observations shown in this paper is the ability to provide safety information for instrumented aircraft and Unattended Aerial Platforms (UAS) since these aircraft are being considered for overpasses of hurricanes that contain deep convection. Section 4 will discuss implications of the observational findings on mixing processes in the tropical tropopause layer. Finally, a summary of our findings along with general conclusions is presented in section 5.

## 2. Convection cases and analysis methodology

### *a. EDOP measurements*

The NASA ER-2 Doppler Radar (EDOP) flying on the high-altitude (~20 km) ER-2 aircraft, is the primary instrument used for this study. EDOP is an X-band (9.6 GHz)

Doppler radar with dual 3$^{o}$ beam width and two antennas, one is fixed at nadir and the other is 30$^{O}$ forward of nadir (Heymsfield et al. 1996). Processed reflectivity and Doppler velocity are obtained every 0.5 s, which corresponds to approximately 100 m of aircraft translation (aircraft ground speed ~ 200 - 210 m s$^{-1}$). This configuration oversamples typical convective cores, but is implemented to allow for better aircraft motion corrections to the Doppler velocities. The footprint of the nadir beam is ~1.1 km (0.55 km) at the surface (10 km altitude), so the effective resolvability is approximately a few hundred meters at 10 km altitude, and 0.5 km near the surface. The profiled Doppler velocities and reflectivities were obtained at 37.5 m (75 m prior to 1997) intervals in the vertical. The Nyquist velocity is ~ 34 m s$^{-1}$ so unfolding was not required. The main editing on raw Doppler velocities was removing noisy data by using a power threshold and corrections for aircraft motions. The aircraft motions are removed from the raw Doppler velocities using the ER-2 inertial navigation system (INS) and the antenna tilt angles. Details of these procedures can be found in Heymsfield et al. (1999, 2001, and 2006).

The reflectivity data have been calibrated to within about 1 dBZ by internal and external calibrations, and checked against the ocean surface return. The minimum detectable reflectivity of EDOP varied between data sets (mainly by year): -10 dBZ at 10 km range (10 km altitude) from 1995– 1997, and -10 dBZ at 10 km range after 1997. Reflectivities were corrected for attenuation using the surface reference approach (Iguchi and Meneghini 1994). The correction was not always performed since EDOP's nadir "surface" receiver channel was not available for all flights and the "rain" receiver channel saturates at the surface. Reflectivity without this correction would result in lower values in the rain region where most of the attenuation occurs. The attenuation correction over land is of lower accuracy since the background (non-precipitating) surface reflectivity returns are more difficult to estimate (Tian et al. 2002).

The Doppler velocities with aircraft motion removed are vertical hydrometeor motions ($v_h$) from which the vertical air motion $w = v_h + v_t$ can be obtained with a hydrometeor fallspeed ($v_f$) assumption based on the reflectivity. The estimates used for $v_f$ are described in more detail in the Appendix where several changes have been made to the fallspeed estimates used in previous studies. Once the fallspeeds are estimated and added to the hydrometeor motions, a median filter is used to remove spurious values and a 9-point (~338 m) running mean is then applied to provide additional smoothing.

*b. Convection cases*

Table 1 lists various NASA field campaigns from 1995-2005 during which the EDOP on ER2 flew above strong convection. These campaigns cover a variety of oceanic and land regions. Further information on the campaigns can be found in the references provided in Table 1. The only non-major campaign in Table 1 was HOPEX conducted primarily for the first EDOP test flights.. The EDOP flight lines were examined for strong convective cells, defined by having either: (1) a strong updraft (> 10 m $s^{-1}$) over at least a kilometer along the flight track, or (2) a 20 dBZ echo extending up to 12 km altitude or greater. Table 2 displays 62 cases of strong to intense convection assembled from different field experiments providing approximate center location and time of each cell, the type of convection, and the field campaign. Hot towers are included from five hurricanes: Bonnie (1998), Georges (1998), Humberto (2001), Dennis (2005), and Emily (2005) and two tropical storms: Chantal (2001) and Gert (2005). Some of these storms have already been analyzed in papers such as Heymsfield et al. (2001, 2006), Geerts et al. 2000, Halverson et al. (2007) and Guimond et al. (2009). Some of the land-based and oceanic cases have been reported in Tian et al. (2002).

Figure 1 shows the locations of the convective events sampled by EDOP sorted into four categories: land (Florida, Brazil, Gulf Coast, Central America), oceanic (Caribbean, Eastern Pacific, Gulf of Mexico), tropical cyclone (Atlantic and eastern Pacific), and sea breeze (Florida). The sea breeze cases were separated from land-based convection since they are likely initiated by different mechanisms than pure oceanic or land-based convection. The location of each case is shown in both the full-scale map and also in the four zoomed panels; symbols in the zoomed panels correspond to cases in Table 2. The cases represent a wide assortment of convection types but they mainly represent the warm season (between June and September) with the exception of the Louisiana cases that were flown during winter. On average, the freezing level for the warm season is at 4.5 - 5 km altitude with the cold season in Louisiana around 3.7 km altitude. Diurnal variations are not considered since the aircraft overpass times vary widely due to both the presence of convection and aircraft safety (landing) issues. This may be an issue in overall generalizations about the data since intense convection often peaks in the afternoon over land with no peak activity over ocean (e.g., Zipser et al. 2006).

*c. Analysis methodology*

As mentioned previously, intense convection in the current study is defined by either a 20 dBZ echo above 12 km altitude, or by updrafts with magnitudes $\geq$10 m s$^{-1}$ at any altitude. There have been many definitions of intense convection as described by Zipser et al. (2006). For example, they defined a strong updraft as having a 40 dBZ echo above 10 km and >10 m s$^{-1}$ velocity above 8 km. The rationale for the case selection in this paper is described below, but was initially based on a subjective appearance of strong, deep convection in the EDOP data with refinement according to the above criteria. It is well known that convection can be comprised of isolated, easily identifiable cells as well as complicated multiple cellular structures in close proximity. In the current study, we do not attempt to separate cells into different stages of development, but we do try to isolate adjacent cells in multicellular situations as much as possible. Convective cells undergo life cycles from growing to mature to dissipating stages. The EDOP cross sections are snapshots during an instant of a convective cell's lifetime. To complicate matters, the lifecycle of vertical velocity and precipitation are not always in phase (i.e., updrafts tend to be strongest during early to mature periods of cell development and precipitation and reflectivities are strongest during the mature and dissipating periods).

In addition to the above, there are other aspects of the EDOP cross sections that will affect interpretations: a) flight tracks may not cross the peak of storm cores or updrafts may be tilted causing only certain levels to be captured; b) strong cross-winds to the ER-2 flight direction from either vertical wind shear or tropical cyclone tangential motions may affect the vertical velocity calculations due to inadequate aircraft motion removal and a cross-wind bias (Heymsfield 1989); c) the selection of flight legs during field campaigns focused on particular events or on strong convection so our data set does not provide a statistical sampling of convection with differing intensities, of diurnal cycle, or seasonal variations. The focus on mean profiles of peak updraft properties in this paper will help reduce some of these sampling uncertainties.

Calculations were performed on cases in Table 2 for various properties of the convection. To simplify the analysis, the EDOP flight lines were zoomed to approximately 10-15 km on either side of the convective core. The hydrometeor fallspeeds were estimated as described in the Appendix, and vertical motion, *w,* was then computed. The zoomed EDOP time-height sections representing the entire convective region with up- and downdrafts were then analyzed for maximum and minimum reflectivity and *w* at each altitude, maximum heights of reflectivity levels (20, 30, 40, 50 dBZ), magnitude and heights of maximum updrafts and downdrafts, widths of updraft cores, radar-derived cloud top height, and other properties derived from other ER-2 instruments. Three examples from Table 2 illustrate the above calculations: intense convection in Rhondonia, Brazil on 25 January 1999 (Fig. 2; Case "V"), Tropical Storm Chantal on 20 August 2001 (Fig. 3; Case "e"), and sea breeze convection along Florida's Atlantic coast on 23 July 2002 (Fig. 4; Case "m"). The cases in Table 2 are quite varied with some cases of strong persistent isolated cells, and others shorter lived with multicellular structure; Figures 2 - 4 show a few varied examples. Panels A - D in Figs. 2-4 show reflectivity, Doppler velocity corrected for air motions, fallspeed, and $w$, with derived quantities superimposed on panels A and D.

Figure 2 resembles a supercell-like tower with a cloud top exceeding 17 km altitude, a 30 dBZ echo at a height of ~16 km, *40* dBZ height at ~6 km, $w_{max}$ at ~12 km altitude, and an updraft width defined by updraft region >5 m s$^{-1}$ at 10 km altitude (v10) of 8-10 km. The is highly attenuated with two-way path-integrated attenuation larger than >40 dBZ (not shown). This tower is among the strongest cases in Table 2. This amount of attenuation is likely an indicator of small hail since 1 cm hail will attenuate an X-band signal about 7 dB km$^{-1}$ (Battan 1973. see page 81 Table 6.5). There is certainly the possibility that the top few cases in this paper have small hail present.

Petersen et al. (2001) examined the variations of convective regimes during TRMM-LBA and their plots show that 40 dBZ echoes rarely get above 8 km altitude, and 30 dBZ contours peak around 14 km. They mention that more intense convection occurs during the easterly regime that was present during this case, but their results are still consistent with the heights in Fig. 2.

Figure 3 from Tropical Storm Chantal has been previously reported in Heymsfield et al. (2006) and Herman and Heymsfield (2003). The 30 dBZ height is lower than that for the previous case, the updraft width is ~5-6 km, and $w_{max}$ and $w_{min}$ again at an altitude above 10 km. More ordinary Florida land-based convection (Fig. 4) has a much narrower updraft and is mostly contains multicellular in nature. It is easy to distinguish two updraft pulses in this cross section, the one on the right has higher reflectivities but the updraft has dissipated, and a new pulse on the left tower has a width of only about 2 km and a strong updraft. Even though there are large dissimilarities between this case and the two previous cases, the general updraft properties of a number of cases are similar as will be seen in the next section.

Vertical profiles in Figs. 5 and 6 show the range of values corresponding to the panels in Figs. 2 and 3. The maximum and minimum, median, and +/-2 σ vertical profiles are plotted for each panel; we have not plotted the full frequency diagram since it was difficult to discern the profile properties. As noted in previous figures, updraft and downdraft maxima are at higher altitudes. Figure 5 indicates an updraft approaching 28 m $s^{-1}$ between 10 and 15 km altitude, and a downdraft of 20 m $s^{-1}$ at 16 km altitude. A second updraft peak of ~17 m $s^{-1}$ is noted at about 5 km altitude. The reflectivity profile exceeds 60 dBZ near the melting level, and drops off to 40 dBZ at 10 km altitude, and remains at ~35 dBZ until about 16 km altitude. A slightly weaker updraft and downdraft is present in Fig. 6 for Tropical Storm Chantal, but more notable is the difference in vertical depth of the intense updraft. The strong downdrafts ~15 m $s^{-1}$ near cloud top at 15 km altitude would at first seem surprising but this has been documented in the literature (Heymsfield and Schotz 1985; Sun et al. 1994) as mentioned earlier. The above two cases clearly show updrafts are strong through the troposphere, but peak values are observed at high storm levels.

**3. General characteristics of convective structure**

To examine general features in Figs 2-6 such as updraft maxima in the upper troposphere, we compare the general characteristics of all cases in Table 2: a) general convection features (Figs. 2-4), b) vertical profiles (Figs. 5 and 6), and c) upper troposphere/ near cloud-top properties since these have implications on satellite measurements and aircraft overflights of convection.

*a. General convection features*

The plots in the following section (Figs. 7-10) have been constructed using quantities calculated similar to those in Figs. 2-4. The panels in each plot are divided into the 4 categories of convection (tropical cyclone, land, oceanic, and sea breeze), and within each category, the points are sorted by location of the data source provided in Table 2. Means are taken within each category. The cases within each category are further sorted so vertical motion maxima increase toward the right. This type of plot allows quick comparison between the diverse set of cases in this study.

1) Vertical velocity maxima and minima (Fig. 7)

Peak vertical velocities range from 9 m $s^{-1}$ to greater than 30 m $s^{-1}$ in panel A. Oceanic and tropical cyclone cases have slightly lower peak vertical velocities than land and sea breeze cases (2 – 5 m $s^{-1}$ in the mean); sea breeze cells had among the strongest updrafts. These updraft magnitudes are not surprising and have been observed previously by *in situ* measurements (Herman and Heymsfield 2003, Jenkins et al. 2008) but they are somewhat higher than that observed by Anderson et al. (2005; maximum value of ~16 m $s^{-1}$) presumably because of aircraft safety concerns with stronger cells. Peak downdrafts (panel B) are also quite strong ranging from a few m $s^{-1}$ to ~15 m $s^{-1}$; the land and sea breeze convection have significantly stronger downdrafts than that of the oceanic or tropical cyclone convection (~17 m $s^{-1}$ versus ~11 m $s^{-1}$ in the mean).

Heights of $w_{max}$ (panel C) occur frequently above 8 km, but they are mainly above 10 km; a few cases have peak updraft below the 8 km level and a few have heights above the 15 km level. The observed vertical motion peak in the upper troposphere can be due to latent heat release by freezing of ice condensate (e.g, Zipser 2003) that produces additional updraft buoyancy, or due to the unloading of hydrometeors in the updraft that reduces the drag on ascending air parcels. Heights of downdrafts $w_{min}$ (panel D) are generally in the upper troposphere with some downdrafts near cloud top; there are a few cases in each category that have downdraft peak heights in the 5 -10 km range. Interestingly, $w_{max}$ heights are 2 km higher in tropical cyclones than other categories, whereas $w_{min}$ heights are 1-2 km lower than other categories. The height of $w_{max}$ is mostly below 10 km for land-based storms (Florida, Continental U.S., and Louisiana winter). This may be a manifestation of drier mid level environments for these cases.

2) Reflectivity level height contours (Fig. 8)

The heights of peak reflectivity of 20, 30, 40, and 50 dBZ, range from ~10-18 km altitude, ~5-17 km, ~3.5-15 km, and 0 -15 km (0 km indicating no 50 dBZ detected in column), respectively. On the average, the heights for oceanic and tropical cyclone cases are generally lower by about 0.5 to 1 km than that of the land and sea breeze categories. Eastern Pacific oceanic storms have lower reflectivities than that of the other oceanic cases. A few hurricane and sea breeze cases have the highest 40 and 50 dBZ heights. Many 50 dBZ heights (Fig. 8, panel D) are at 5-7 km altitude (0 to -10$^{O}$C) suggesting supercooled raindrops are lofted above the freezing level, and freeze near the -10$^{O}$C level. There is approximately a 7 dB increase in the reflectivity between the ice and water phase because of the increase in the dielectric coefficient. This results in sharp decrease in reflectivity above the 5 -6 km level in many of the cases. We will discuss this subject further in section 4.

Three cases were especially strong compared to the others. Sea breeze cases M and N (15 August 1998) had centimeter-size hail based on ground-based S-band polarimetric radar data (Tian et al. 2002). Case t (Hurricane Emily) clearly stands out as well; both storms had 40 dBZ extending up to 14-15 km altitude that fit among the strongest storms in the Zipser et al. (2006) study. The Brazil cases V and W (25 January 1999) has 40 dBZ up to 14-15 km altitude suggesting possible large graupel or hail in this storm but no ground-based radar observations were available.

3) Peak updraft/downdraft and reflectivity at 10 km altitude (Figure 9)

This level is examined since it is near the -40$^{o}$C altitude and it is near the base of the strongest convection. The reflectivity panel A shows a significant variability among the cases with Florida sea breeze convection. Cases M, N clearly have the highest reflectivities (~50 dBZ); this case was previously mentioned to have small hail detected with polarimetric radar. Hurricane Emily (case t) is the next strongest case, followed by a number of land-based storms. The means of maximum reflectivity are ~30-40 dBZ for the convection categories with land and sea breeze having consistently higher values than the oceanic cases. The peak vertical velocities (panel B) also consistently show higher values in the land-based and sea breeze convection. The tropical cyclone cases consistently have ~12 m s$^{-1}$ updrafts with the exception of Tropical Storm Chantal (Figs. 3D and 6D; case e), which contained a 23 m s$^{-1}$ value. This value is reasonable since it is near the value observed by the NASA DC-8 aircraft during the penetration of one of the updrafts in this storm (Herman and Heymsfield 2003). Downdrafts (panel D) have peak values mostly in the 2 – 6 m s$^{-1}$ range with some values between 10 - 14 m s$^{-1}$ indicating that most of the strongest downdrafts occur above 10 km altitude (compare with Fig. 7B).

4) Widths of reflectivity cores at 6, 8, and 12 km altitude (Figure 10)

It is very difficult to obtain the width of the reflectivity core profiles so we have examined widths at discrete levels as previously defined in Figs. 2-4; it is even more difficult to obtain width of the updraft core since the updrafts are more transient and the passes may not be across the maximum width. The 45 dBZ widths at 6 km altitude and 35 dBZ widths at 8 km altitude range from ~0.5 - 8 km, with land-based cores significantly wider than that for the oceanic and tropical cyclone categories (~4 - 5 km versus ~1.8 km). The width of the 20 dBZ core at 12 km, the upper level anvil outflow, also has considerable variability in core width (~0.5 - 9 km), but all widths have broadened to ~5 - 6 km in the mean. Anderson et al. (2005 and references therein) found that updraft cores (based on vertical velocities) during various tropical field programs had median widths of ~1 km and top 10% core widths from ~1.5 – 4 km (~4 – 6 km) for non-hurricane (hurricane) cases; core widths increased slightly with height from near surface to 9 km altitude. Their cases were biased toward weaker updrafts that could safely be penetrated by aircraft, but observations here are reflectivity core width that would be expected to be larger and less well-defined than vertical velocity. EDOP-derived widths in this paper may also be exaggerated since the radar beam acts much like a filter so features less than the beamwidth may be smeared out.

*b. Vertical profiles*

Vertical profiles of reflectivity, updrafts, and downdrafts sorted by convection class are shown in Figs. 11-13. These profiles were constructed using peak values (e.g., rightmost curves in Figs. 5A, 5D, 6A, 6D. Each curve is from a different case in Table 2, and the curves were sorted by convection category; individual curves are not identified by case since it would be difficult to discern in the figure; the bold black curves are the mean curve for each class. All reflectivity profiles (Fig. 11) show a strong decrease with increasing altitude above the freezing level. Two extreme cases (case N and t on the rightmost curves in oceanic and tropical cyclone panels) have significantly higher reflectivities aloft. The mean profiles show that the land profile is a few dB higher than all the other profiles, and the oceanic profile is the smallest of all other profiles. Szoke et al. (1986) compared reflectivity profiles of GATE tropical convection, New England showers, and hurricanes (see their Fig. 12) and have shown a similar decrease of reflectivity with increasing height. Hail and tornadic storms were the only profiles with 50 dBZ from the surface to the freezing level, and 50 dBZ reached 10 km altitude only for tornadic storms. Profiles in Fig. 11 in general have much higher reflectivities possibly due to the higher resolution of the aircraft measurements as well as a higher accuracy calibration. There is not as significant a difference in the reflectivity profiles as would be expected with convection of different types and locations. One very interesting observation is that the reflectivities in the majority of cases decrease rapidly above 5 or 6 km altitude, where 6 km is roughly the -10$^{o}$C level. Stith et al. (2002, 2004) found from *in situ* measurements in the Amazon and Kwajalein that most of the updrafts glaciated rapidly removing most of the supercooled liquid water between -5 to -17$^{o}$C. This is consistent with our observations since reflectivities will be much lower in the ice phase as mentioned earlier.

The peak vertical velocity profiles (Fig. 12) show large variability in mid to upper levels, for all convection classes. The height of the maximum vertical velocities in the oceanic and tropical cyclone profiles are generally higher than that of the land and sea breeze convection cases as noted earlier. The mean profiles depict an increase of vertical velocity from a few meters per second near the surface to ~10 m s$^{-1}$ at 5 km altitude (~0$^{o}$C), a minimum near 6 – 7 km altitude, and then another increase up to the maximum in the profile above 10 km altitude (except for the oceanic profile that has a dip to 10 m s$^{-1}$ at 10 km altitude). The updrafts vary widely in behavior in part due to capturing them at various stages of the storms lifetime. We will discuss their general behavior in section 4.

The downdrafts in Fig. 13 are more widely varied than the updrafts. The mean downdraft in the land and oceanic cases increase with altitude from about 5 m $s^{-1}$ near the surface to 8-10 m $s^{-1}$ near the 15 km level; the peak downdrafts in tropical cyclones are more uniform with height with a mean value of approximately 6-7 m $s^{-1}$. There were some very strong downdrafts in the tropical cyclone cases. A few of the land convection cases had extremely large downdrafts that are suspicious since this was from one of the oldest data sets among the first EDOP measurements.

c. *Satellite implications*

Satellite studies of deep convection using TRMM observations have used the height of reflectivity contours as a proxy for convection intensity (e.g. Zipser et al. 2006 and references therein). Intensity of convection is largely based on updraft strength but this is not available from satellite measurements. Figure 13 provides plots for the 30 and 40 dBZ echo height (Figs. 13A, B) versus maximum updraft strength. Our sample is biased toward strong to intense convection but the plots show some correlation 0.5 (0.6) for 30 (40) dBZ, but with considerable scatter likely due to the life cycle of the convection. Nevertheless, when 30 dBZ echoes are at or above 10 km altitude, it is likely that the updrafts are at least 10 - 12 m $s^{-1}$, if not significantly stronger. When the 40 dBZ echo is above 10 km, most of the updrafts are >15 m $s^{-1}$. This is useful information for the TRMM Precipitation Radar since it attaches some significance of using reflectivity heights as a proxy for updraft strength.

## 4. Discussion of convection statistics

The mean profiles of peak values for the different classes of convection are summarized in Fig. 15 that compares the mean profiles of peak values for the different classes of convection. The most notable differences in the figure are the following a) the oceanic reflectivity profile is at least 5 dBZ lower than that of the other reflectivity profiles; b) the tropical cyclone convection vertical velocities are lowest in mid-levels but still have comparable maxima to all other cases except the land-based convection; and c) the updrafts increase to about 10 m $s^{-1}$ near the melting level and they are very similar between cases. These observations pose several very interesting questions related to the dynamics and microphysics of tropical convection: a) Why do the updraft peaks often have a bimodal structure with a low-level (<6 km) and upper-level (>10 km) peak? and b) Why are the updraft maxima are often above 10 km altitude? Work by Zipser (2003) and Fierro et al. (2009) suggest that latent heating produced by freezing of supercooled liquid hydrometeors at temperatures well above the freezing level provides a boost to the updraft that may be responsible for higher updraft speeds aloft. Fierro et al. (2009) studied this process using the Weather Research and Forecast (WRF) model and suggested that the original hot tower hypothesis that postulated undiluted towers should be modified to include mixing. They further suggest that the boost from latent heat compensates the effects of mixing at lower levels.

The microphysics is critical toward understanding the above questions. Heymsfield et al. (2009) used an assemblage of in situ penetrations of maritime updrafts and showed that most of the condensate is removed before reaching the -20$^{o}$C level in low latitude updrafts and the amount continues to diminish upward in the updrafts. They further suggest that even with vigorous updrafts, large ice sediments through and out of the updrafts. The reflectivity profiles in Fig. 11 further support this view. The decrease of the reflectivity with height implies a decrease in ice water content similar to that observed in Heymsfield et al. (2009) suggesting significant fallout or loss of hydrometeor mass with altitude.

With this in mind, the general behavior of the observed updraft profiles can be described as follows. As raindrops grow above cloud base while ascending to the $0^{o}$C level (or -$10^{o}$C level if supercooled), latent heating from condensation provides buoyancy for the updraft. Drag from rain progressively loads down the updrafts with height just above the $0^{o}$C level, as suggested by the slight minima observed in the observations (Fig. 15) just above the $0^{o}$C level (5 to 6 km). Updrafts strengthen above 6 – 7 km after the fall out of hydrometeors which reduced the precipitation load in the updraft. The freezing of remaining supercooled water latent heating due to growth of the ice and ice nucleation occurs up to the homogeneous nucleation level (~$36^{o}$C, ~10 km) resulting in additional updraft buoyancy. The complexity of these processes requires further study since there are several competing processes that require better observations and improvements in microphysics parameterizations in the numerical models.

## 5. Summary and conclusions

This paper has presented vertical motion and reflectivity structure from a diverse set of multi-year observations of convection from NASA field experiments in the tropics and subtropics. The measurements were obtained from the nadir-viewing EDOP radar on the high-altitude NASA ER-2 aircraft. This study is the first time that updrafts, particularly oceanic, have been examined in such detail through their full vertical extent. Four types of convection were defined in the paper (tropical cyclone, land-based, oceanic, and sea breeze) based on the cases studied. A number of interesting features were obtained from the analyses of reflectivity and vertical motions providing insights on the kinematic and microphysical processes that are otherwise difficult to obtain.

It was found that both updrafts and downdrafts in deep land-based and oceanic convective storms are quite strong with peak updraft values often exceeding 15 m $s^{-1}$ and the height of the peak often above 10 km altitude; sometimes a second smaller peak in the vertical velocity was present near the freezing level. The land-based and sea breeze storms had slightly stronger updrafts than the oceanic and tropical cyclone convection cases. The heights of peak updrafts for tropical cyclones were 1 - 2 km higher than that of the other convection types. The reflectivity profiles showed that oceanic convection had lower reflectivities in general compared to other classes of convection; one tropical cyclone and one sea breeze case clearly stood out from the other cases as being extreme. The tropical cyclone convection had peak updrafts at about the 12 km level, a few kilometers higher than that for the other convection types. But the tropical cyclone cases had the weakest mid-level updrafts.

Vertical velocity is a key unknown measurement from the TRMM and future GPM satellites whose mission is not only to measure tropical rainfall, but also to estimate heat budgets in precipitation. In this study, we used the reflectivity and vertical motions to explore the relationship between high reflectivities aloft and the strength of updrafts. A correlation of 0.6 (0.5) was found between the height of the 40 dBZ (30 dBZ) reflectivity and vertical velocity. It is likely that this lack of correlation in some cases is due to the phasing of the reflectivity and vertical motion, i.e., the peak updrafts often occur during early development of cells, and the peak reflectivities occur during the mature to dissipating stages of the cell. This has implications on satellite retrievals that capture an instant during the lifetime of a convective event. It would appear that intensity estimates from convection with weaker reflectivities over land by TRMM would be more difficult and furthermore, latent heating estimates based on these have much larger uncertainties.

This study has focused mainly on characterizing the radar measurements and not on the convective environment (i.e., convective available potential energy – CAPE, vertical shear, or other pertinent parameters). We have not presented discussion on entrainment in this paper even though the peak updraft profiles suggest strong convergence and possibly entrainment in midlevels. These subjects will be explored in future efforts through a more rigorous examination of the dynamics and microphysics that produce the general behavior of the observed updraft and reflectivity profiles. Finally, the vertical velocity magnitudes at higher altitudes near the storm top are quite strong suggesting safety concerns for high altitude UAS such as the Global Hawk that will fly near the 18 km altitude level for hurricane reconnaissance. Convection frequently overshoots the tropopause in a number of the cases studies, with altitudes reaching 15 – 18 km.

**Acknowledgements**

This work was mostly supported by NASA's Atmospheric Dynamics Program although some of the data collection and analysis were sponsored by the NASA Radiation Sciences Program (Crystal-Face and TC4). We are greatly appreciative of Jeff Caylor, Steve Bidwell, Ed Zenker and Larry Belcher, and others for the many years of hard work on the radar hardware and data processing required for obtaining the high-quality data sets in this study.

**References**

Adler, R. F., and R. A. Mack, 1986: Thunderstorm cloud top dynamics as inferred from satellite observations and a cloud top parcel model. *J. Atmos. Sci.*, **43**, 1945-1960.

Anderson, N. F., C. A. Grainger, and J. L. Stith, 2005: Characteristics of strong updrafts in precipitation systems over the Central Tropical Pacific Ocean and the Amazon. *J. Appl. Meteor.*, **44**, 731-738.

Battan, L. J., 1973: Radar Observation of Atmosphere. University of Chicago Press, 324 pp.

Beard, K. V., 1976: Terminal velocity and shape of precipitation and cloud drops aloft. *J. Atmos. Sci*., **33**, 851-864.

_________, 1985: Simple altitude adjustments to raindop velocities for Doppler analysis. *J. Atmos. Ocean. Tech.*, **2**, 468-471.

Black, R. A., H. B. Bluestein, and M. L. Black, 1994: Unusually strong vertical motions in a Caribbean Hurricane. **Mon. Wea. Rev.**, *122*, 2722-2739.

________, G. M. Heymsfield, and J. Hallett, 2003: Extra large particle images at 12 km in a hurricane eyewall: Evidence of high-altitude supercooled water? Geophys. Res. Let., doi:10.1029/2003GL017864

Black, P. G., R. A. Black, J. Hallett, and W. A. Lyons, 1986: Electrical activity on the hurricane. Preprints, 23rd Conf on Radar Meteorology, Snomass, CO, AMer. Meteor. Soc., J277-J280.

Black, M.L., R. W. Burpee, and F. D. Marks, Jr., 1996: Vertical motion characteristics of tropical cyclones determined with airborne Doppler radial velocities. *J. Atmos. Sci*., **53**, 1887-1909.

Bohren, C.F., and D. R. Huffman, 1983: Light Scattering by Small Particles, Wiley, New York.

Cecil, D.J., S.J. Goodman, D.J. Bocippio, E.J. Zipser, and S.W. Nesbitt, 2005: Three years of TRMM precipitation features. Part I: Radar, radiometric, and lightning characteristics. *Mon. Wea. Rev*., **133**, 543-566.

Fierro, A. O., J. M. Simpson, M. A. Lemone, and J. M. Straka, 2009: On how hot towers fuel the Hadley Cell: An observational and modeling study of line-organized convection in the Equatorial Trough from TOGA COARE. *J. Atmos. Sci.*, submitted.

Foote, G. B., and P. S. Du Toit, 1969: Terminal velocity of raindrops aloft. *J. Appl. Meteor*, **8**, 249-253.

Geerts, B., G. M. Heymsfield, L. Tian, J. B. Halverson, A. Guillory, and M. I. Mejia, 2000: Hurricane Georges's landfall in the Dominican Republic: Detailed airborne Doppler radar imagery. *Bull. Amer. Meteor. Soc.*, **81**, 999-1018.

Guimond, S.R., G.M. Heymsfield and F.J. Turk, 2009: Multi-scale observations of Hurricane Dennis (2005): The effects of hot towers on rapid intensification. *J. Atmos. Sci*., submitted.

Halverson, J., and coauthors, 2007. NASA's Tropical Cloud Systems and Processes Experiment-Investigating tropical cyclogenesis and hurricane intensity change. *Bull. Amer. Meteor. Soc.*, **88**, 867-882.

Herman, R.L., A.J. Heymsfield, 2003: Aircraft icing at low temperatures in Tropical Storm Chantal (2001). *Geophys. Res. Lett.*, doi: 10.1029/2003GL017746.

Heymsfield, A.J., A. Bansemer, C. Schmitt, C. Twohy, and M. R. Poellot, 2004: Effective ice particle densities derived from aircraft data. J. Atmos. Sci., 61, 982-1003.

____________, L. M. Miloshevich, C. Schmitt, A. Bansemer, C. Twohy, M. R. Poellot, A. Fridland, and H. Gerber, 2005: Homogeneous ice nucleation in subtropical and tropical convection and its influence on cirrus anvil microphysics. *J. Atmos. Sci.,* **62**, 41-64.

______________, A. Bansamer, G. Heymsfield, A. Fierro, 2009: Microphysics of maritime tropical convective updrafts at temperatures from -20 to -60$^{O}$C. Submitted, J. Atmos. Sci.

Heymsfield, G. M. and S. Schotz, 1985: Structure and evolution of an Oklahoma squall line, *Mon. Wea. Rev.*, **113**, 1563-1589.

_____________, 1989: Accuracy of vertical air motions from nadir viewing Doppler airborne radars. *J. Atmos. Oceanic Tech.*, **6,** 1079-1082.

____________, R. Fulton, and J. Spinhirne, 1991: Aircraft overflight measurements of Midwest severe thunderstorms: Implications on geosynchronous Satellite interpretations, *Mon. Wea. Rev.*, **119**, 436-456.

____________, S. Bidwell, I. J. Caylor, S. Ameen, S. Nicholson, W. Boncyk, L. Miller, D. Vandemark, P. E. Racette, and L. R. Dod, 1996: The EDOP radar system on the high altitude NASA ER-2 Aircraft, *J. Atmos. Oceanic Tech*., **13**, 795-809.

____________, J.B. Halverson, and I. J. Caylor, 1999: A wintertime Gulf coast squall line observed by EDOP airborne Doppler radar. *Mon. Wea. Rev.*, **127**, 2928-2950.

____________, J. B. Halverson, J. Simpson, L. Tian, P. Bui, 2001 ER-2 Doppler Radar (EDOP) Investigations of the Eyewall of Hurricane Bonnie During CAMEX-3, *J. Appl. Meteor.*,, **40**, 1310-1330.

____________, J. Halverson, E. Ritchie, J. Simpson, J. Molinari, and L. Tian, 2006: Structure of highly sheared tropical storm Chantal during CAMEX-4. *J. Atmos. Sci.*, **63**, 268-287.

Houze, R. A., Jr., W.-C. Lee, M. M. Bell, 2009: Convective Contribution to the Genesis of Hurricane Ophelia (2005), In press, Mon. Wea. Rev. 2009.

Hou, A.Y., R.K. Kakar, S. Neeck, A. A. Azarbarzin, C. D. Kummerow, M. Kojima, R. Oki, K. Nakamura, T. Iguchi, 2009: The Global Precipitation Measurement (GPM) Mission. Submitted to Bull. Amer. Meteor. Soc.

Iguchi, T., and R. Meneghini, 1994: Intercomparison of single frequency methods for retrieving a vertical rain profile from airborne or spaceborne radar data. J. *Atmos. Oceanic Technol*., **11**, 1507-1516.

Jenkins, G.S., A, Pratt, and A. Heymsfield, 2008: Possible linkages between Saharan dust and Tropical Cyclone Rain Band Invigoration in Eastern Atlantic during NAMMA-06. *Geophys. Res. Lett.,* **35,** L08815, doi:10.1029/2008GL034072

Jensen, E., D. Starr, and O. Toon, 2004: Mission investigates tropical cirrus clouds. *EOS Transactions, AGU*, **85**, 45-50.

Jorgensen, D. P., E. J. Zipser, and M. A. LeMone, 1985: Vertical motions in intense hurricanes. *J. Atmos. Sci*., **42**, 839-856.

____________, and M. A. LeMone, 1989: Vertical velocity characteristics of oceanic convection. *J. Atmos. Sci*., **46**, 621-640.

Kakar, R., M. Goodman, R. Hood, and A. Guillory, 2004. Overview of the Convection and Moisture Experiment (CAMEX), *J. Atmos. Sci.*, **63**, 5-18.

Knight, C. A., and A. J. Heymsfield, 1983: *J. Atmos. Sci.*, **40**, 1510.

Lang., S., W.-K. Tao, R. Cifelli, W. Olson, J. Halverson, S. Rutledge, and J. Simpson, 2007: Improving simulations of convective systems from TRMM LBA: Easterly and westerly regimes. J. Atmos. Sci., 64, 1141-1164.

Lemone, M. A., and E. J. Zipser, 1980: Cumulonimbus vertical velocity events in GATE. Part I: Diameter, intensity and mass flux. *J. Atmos. Sci*., **37** 2444-2457.

Lin, Y.-L., R. D. Farley, and H. D. Orville, 1983: Bulk parameterization of the snow field in a cloud model. J. Appl. Meteor., 22, 1065-1092.

Liu, C., and E. J. Zipser, 2005: Global distribution of convection penetrating the tropical troposapuse. J. Geophys. Res., **110**, D23104, doi:10.1029/2005JD006063.

Lucas, C., M.A. LeMone, and E. J. Zipser, 1994: Vertical velocity in oceanic convection off tropical Australia. *J. Atmos. Sci.*, **51**, 3183-3193.

Marks, F. D., and R.A. Houze, Jr, 1987: Inner core structure of Hurricane Alicia from airborne Doppler radar observations, *J. Atmos. Sci*., **44**, 1296-1317.

Mitchell, D. L., and A. J. Heymsfield, 2005: Refinements in the treatment of ice particle terminal velocities, highlighting aggregates. *J. Atmos. Sci.*, 62, 1637–1644.

Montgomery, M. T., M. E. Nicholls, T. A. Cram, and A. B. Saunders, 2006: A vertical hot tower route to tropical cyclogenesis. *J. Atmos. Sci*., **63**, 355-386.

Nesbitt, S.W., E.J. Zipser, and D. J. Cecil, 2000: A census of precipitation features in the Tropics using TRMM: Radar, ice scattering, and ice observations. *J. Climate*, **13**, 4087-4106.

Petersen, W.A., and S.A. Rutledge, 2001: Regional variability in tropical convection: Observations from TRMM. *J. Climate*, **14**, 3566-3586.

Pflaum, J. C., and H. R. Pruppacher, 1978: A wind tunnel investigation of graupel initiated from frozen drops. *J. Atmos. Sci.*, **36**, 680-689.

Sherwood, S. C., and A.E. Dessler, 2000: On the control of stratospheric humidity. *Geophys. Res. Lett.*, **27**, 2513-2516.

Simpson, J., and V. Wiggert, 1969: Models of precipitating cumulus towers. *Mon. Wea. Rev.*, **97**, 471-479.

__________., C. Kummerow, W.-K. Tao, and R. F. Adler, 1996: On the Tropical Rainfall Measuring Mission (TRMM). *Meteor. Atmos. Phys.,* **60,** 19–36.

___________, J.B. Halverson, B. S. Ferrier, W. A. Petersen, R.H. Simpson, R. Blakeslee, and S. L. Durden, 1998: On the role of "hot towers" in tropical cyclone formation, *Meteorology and Atmos. Physics*, **67**, 15-35.

Starr, D.O'C., 2008: Probing the Mysteries of the Tropopause Transition Layer: The TC4 Experiment. Earth Observer, 20 (3), 22-27. [Available from EOS Project Science Office homepage, http://eospso.gsfc.nasa.gov/

Stith, J.L., J.E. Dye, A. Bansemer, and A.J. Heymsfield, C.A. Grainger, W.A. Petersen, and R. Cifelli, 2002: Microphysical Observations of tropical clouds. *J. Appl. Meteor.*, **41**, 97-117.

_________, J.A. Haggerty, A. Heymsfield, and C.A. Grainger, 2004: Microphysical characteristics of tropical updrafts in clean conditions. *J. Appl. Meteor.*, **43**, 779-794.

Stommel, H., 1947: Entrainment of air into a cumulus cloud, *J. Meteor.*, **4**, 91-94.

Sun, J., S. Braun, M.I. Biggerstaff, R.G. Fovell, and R.A. Houze, Jr., 1994: Warm upper-level downdrafts associated with a squall line. *Mon. Wea. Rev*., **121**, 2919-2927.

Szoke, E.J., E. J. Zipser, and D. P. Jorgensen, 1986: A radar study of convective cells in mesoscale systems in GATE. Part I: vertical profile statistics and comparison with hurricanes. J. Atmos. Sci., 43, 182-196.

Tian, L., G. M. Heymsfield, and R. C. Srivastava, 2002: Measurements of attenuation with airborne and ground-based radar in convective storm over land and its microphysical implications. *J. Appl. Meteor.*, 41, 716-733.

Ulbrich, C.W., and P.B. Chilson, 1994: Effects of variations in precipitation size distribution and fallspeed law parameters on relations between mean Doppler fallspeed and reflectivity factor. *J. Atmos. Ocean. Tech*., **11**, 1656-1663.

Zipser, E. J., 2003: Some view on "hot towers" after 50 years of tropical field programs and two years of TRMM data. Cloud Systems, Hurricanes, and the TRMM. Meteorological Monographs, **51.**

__________, D. J. Cecil, C. Liu, S. W. Nesbitt, and D. P. Yorty, 2006: Where are the most intense thunderstorms on Earth? Bull. Amer. Meteor. Soc., 1057-1071.

Appendix A. Fallspeed Calculations

Calculation of vertical velocity $w$ from EDOP nadir $v_d$ observations requires estimation of the reflectivity weighted fall velocity $v_t$ at each grid point as in Heymsfield et al. (1999; hereafter H99). The $v_t$ estimation is the most critical assumption in obtaining $w$ since $v_t$ depends on many factors such as particle phase, particle size distribution, ice particle habit, etc. In H99, stratiform regions are separated vertically into three regions: rain, snow, and transition region corresponding to the melting layer. The approach is modified from previous papers (Marks and Houze 1987, Black et al. 1996) that uses *reflectivity* -$v_t$ relations relations for the snow, rain, transition (melting), and convective regions. The H99 approach was modified for EDOP observations using a more realistic rain *reflectivity*-$v_t$ relation derived for a gamma distribution (Ulbrich and Chilson 1994) and using a parabolic profile in the transition region instead of a linear. Here we make two additional changes to provide more realistic fallspeed assumptions: 1) a revised fallspeed relation for snow and graupel since higher density, higher fallspeed graupel was not considered in previous papers, and 2) account for the occurrence of supercooled raindrops in strong updrafts.

Difficulties with fallspeed estimation occur in mixed phase regions associated with convection where strong updrafts can loft liquid water, frozen rain, and graupel several kilometers above the melting level. In situ aircraft are often unable for safety reasons to fly through strong convection where graupel and hail may be present. Black et al. (1986) documented hurricane microphysics with the WP-3D aircraft and found that convection was almost completely glaciated above the -5$^{o}$C level and that millimeter-diameter graupel was common. Black et al. (2003) observed from probe data 2 -3 mm spherical particles at 12 km altitude (-40$^{o}$C) in a hot tower in Hurricane Bonnie. These particles were suggested to be a mixture of ice and some supercooled raindrops. Raindrops for this size and altitude would have fallspeeds of ~13 m s$^{-1}$ at 12 km altitude. Herman and Heymsfield (2003) found millimeter-size slushy particles in Tropical Chantal also near the -40$^{o}$C level. Previous tropical and hurricane observations do not indicate high density ice, i.e., hail, so it is not considered in the current study since it is unlikely that it is present in the majority of the cases presented.

The snow fallspeeds previously used are underestimates for graupel, that can have significantly higher fallspeeds, resulting in *w* errors of several meters per second or more in convective regions. An additional problem is that raindrops that contribute significantly in the reflectivity-weighted fallspeed, may freeze above the freezing level at -10 or -20$^{o}$C (6-8 km altitudes). Stith et al (2002, 2004) found that significant supercooled water was found at temperatures warmer than -12$^{o}$C in strong updrafts, although some was found at temperatures as cold as -18$^{o}$C. Most large drops freeze by -10$^{o}$C and the cloud drops freeze at the lower temperatures they observed. Based on these more recent microphysical observations, the H99 fallspeed estimates are modified with a) an improved fallspeed relation for the ice phase, and b) more realistic representation of the raindrop freezing level in strong convection.

The fallspeeds for the ice phase, $v_i$, are derived from a combination of in situ measurements for snow derived from CRYSTAL-FACE (C-F) convection measurements in Florida (Heymsfield et al. 2004) and theoretical calculations for graupel based on limited observations. For the snow calculations, in situ measurements were used from all cases during C-F that consisted of an assortment of stratiform and convection cases maritime and over land. Calculations were made based on Mie spheres using C-F size distributions and size-dependent mean densities constrained by IWC measurements. Snow fallspeeds $v_S$ were then calculated based on Mitchell and Heymsfield (2005) and particle area measurements and densities derived from the in situ measurements. Calculated 9.6 GHz Doppler velocities versus reflectivity are shown Figure A1a for all C-F cases for the 1000 hPa (surface) pressure, where the reflectivities range from less than -10 dBZ to 29 dBZ. A linear curve (-3.4 + 0.19 dBZ) is fitted to the snow points as shown in the figure.

The graupel fallspeeds $v_G$ were calculated based on previous theory and limited observations. Size distrbutions are taken to be exponentials, $N = N_0 e^{-\lambda D}$, where $N_0$ is taken as 0.1 or 0.01 cm$^{-3}$ (Lin et al. 1983), $D$ is particle diameter, and $\lambda$ is the slope of the size distribution. $N_0$ is taken to be 0.01 cm $^{-4}$ as a lower bound. Ice density ($\rho$) at temperatures below -10$^{O}$C have been assumed 0.15 g cm$^{-3}$ found as the ensemble mean for heavily rimed particles for a typical C-F updraft (Heymsfield et al. 2005), 0.4 g cm$^{-3}$ from wind tunnel observations of Pflaum and Pruppacher (1979) and Knight and Heymsfield (1983), and 0.25 g cm$^{-3}$ as an intermediate value. For an exponential distribution, $IWC=N_0\,\rho\Gamma(4)/\lambda^4$. IWC is specified from 0.01 to 2 g cm$^{-3}$ based on C-F observations, and $N_0$ is adjusted to give the correct IWC with the addtition of a maximum diameters $D_{max}$ assumption chosen as: 0.5, 0,8, 1.2 and 2 cm from C-F and other observations. Radar reflectivity is calculated at 9.6 GHz (EDOP frequency) using Bohren and Huffman (1983) Mie scattering equations for spherical ice hyrdrometeors. Figure A1a shows the relations calculated for the various $D_{max}$, $N_0$, and ρ above. A linear curve is fitted through IWC = 1 $gm^{-3}$ points on each of the graupel curves.

The above relations for $v_S$ and $v_G$ applies to ground level (1000 hPa); fallspeeds at other altitudes is obtained by multiplying by $[\rho_o/\rho]^x$ where ρ and $\rho_o$ are the air density at the surface and measurement height, respectively, and *x* varies from 0.4 to 0.45 depending on rain rate and other factors (Beard 1976, 1985); here we assume 0.45. The above fallspeed relations are at the surface and must be multiplied by this correction factor. The Jordan mean tropical sounding was used for all cases except the HOPEX Louisiana convection winter cases; nearby sounding were used for these mid-latitude cases where the freezing level was at approximately 3.2 km.

$(\rho/\rho_o)^{0.44}$, where r and $r_o$ are the densities of air at the level of the observation site and sea level, respectively (Foote and du Toit 1969).

Figure A1b shows the three fallspeed curves ($v_R$, $v_S$, and $v_G$) used in the paper. Also shown are a few other well-referenced fallspeed curves for comparison. A diagram describing the calculation of reflectivity-weighted fallspeed estimates is given in Figure A2. The main changes here from H99 are the $v_i$ calculation and the transitioning between rain and snow or graupel between 6 and 8 km in convective cores. Using the curves in Fig. A1b for the EDOP fallspeed correction would likely have an uncertainty less than 1-2 m $s^{-1}$ based on the above discussion. It is unlikely that this fallspeed uncertainty would affect the results in this paper since the vertical velocities in the updrafts and downdrafts are significantly larger than a few meters per second.

Table 1. Field campaigns with overflights by EDOP.

| Field Campaign | Acronym | Date | Objectives | Reference |
|---|---|---|---|---|
| Houston Precipitation Experiment | HOPEX | Jan 1995 | EDOP test flights | Heymsfield et al. (1999) |
| Convection and Moisture Experiment-2 | CAMEX-2 | Aug-Sept 1995 | convection, water vapor | Heymsfield et al. (1996b) |
| Convection and Moisture Experiment-3 | CAMEX-3 | Jul - Sept 1998 | convection, tropical storms, TRMM validation | Kakar et al. (2004) |
| TRMM Large Scale Biosphere - Atmosphere Experiment | TRMM-LBA | Jan-Feb 1999 | precipitation systems, convection, TRMM validation | http://disc.sci.gsfc.nasa.gov/fieldexp/TRMM_FE/lba/ |
| Convection and Moisture Experiment-4 | CAMEX-4 | Aug -Sept 2001 | convection, tropical storms, TRMM validation | Kakar et al. (2004) |
| Cirrus Regional Study of Tropical Anvils and Cirrus Layers - Florida Area Cirrus Experiment | CRYSTAL-FACE | Jul 2002 | tropical cirrus, aerosols, chemistry, EOS validation | Jensen et al. (2004) |
| Tropical Cloud Systems and Processes | TCSP | Jul 2005 | tropical storms, convection | Halverson et al. (2007) |
| Tropical Composition, Cloud and Climate Coupling | TC4 | Jul 2005 | tropical cirrus, aerosols, chemistry | Starr (2008) |

Table 2. Convection cases. Categories of convection: L (land), T (tropical cyclone), O (oceanic), S (sea breeze).

| ID | DATE | TIME | LAT | LON | DESCRIPTION | CAMPAIGN | CATEG |
|---|---|---|---|---|---|---|---|
| A | 950106 | 20:46:19 | 30.43 | -89.77 | Mississippi winter | HOPEX | L |
| B | 950106 | 20:57:47 | 29.38 | -90.47 | Louisiana winter | HOPEX | L |
| C | 950106 | 22:19:16 | 29.92 | -89.31 | Louisiana winter | HOPEX | L |
| D | 950106 | 22:21:18 | 29.71 | -89.40 | Louisiana winter | HOPEX | L |
| E | 950826 | 21:33:40 | 33.26 | -79.25 | S Carolina land | CAMEX2 | L |
| F | 950826 | 22: 0:47 | 34.36 | -82.62 | S Carolina land | CAMEX2 | L |
| G | 950826 | 22:11:35 | 33.89 | -83.77 | S Carolina land | CAMEX2 | L |
| H | 950828 | 22: 8:46 | 34.67 | -73.58 | N Carolina Atlantic Ocean | CAMEX2 | O |
| I | 950828 | 23: 7:59 | 30.79 | -78.09 | SC/Georgia Atlantic Ocean | CAMEX2 | O |
| J | 950828 | 23: 9:11 | 30.93 | -78.06 | SC/Georgia Atlantic Ocean | CAMEX2 | O |
| K | 980808 | 17:35:56 | 27.38 | -80.92 | Florida land | CAMEX3 | L |
| L | 980808 | 17:49:34 | 27.43 | -80.93 | Florida land | CAMEX3 | L |
| M | 980815 | 22:28:44 | 28.27 | -81.06 | Florida sea breeze | CAMEX3 | S |
| N | 980815 | 22:37:48 | 28.15 | -81.09 | Florida sea breeze | CAMEX3 | S |
| O | 980823 | 19:59: 2 | 24.61 | -71.36 | Hurricane Bonnie Cat. 3 | CAMEX3 | T |
| P | 980824 | 22:30:54 | 26.73 | -72.67 | Hurricane Bonnie Cat. 3 | CAMEX3 | T |
| Q | 980905 | 22:20: 2 | 28.74 | -82.05 | Florida land | CAMEX3 | L |
| R | 980917 | 19:24:54 | 27.65 | -85.16 | Gulf of Mexico (FL) | CAMEX3 | L |
| S | 980917 | 19:47:17 | 26.68 | -83.96 | Gulf of Mexico (FL) | CAMEX3 | L |
| T | 980921 | 17:21: 4 | 17.66 | -64.46 | Hurricane Georges Cat. 2 | CAMEX3 | T |
| U | 980922 | 23:18:29 | 18.82 | -70.65 | Hurricane Georges Cat. 2 | CAMEX3 | T |
| V | 990125 | 22:21:22 | -12.27 | -61.88 | Brazil Rhondonia | LBA | L |
| W | 990125 | 22:43:34 | -12.35 | -62.05 | Brazil Rhondonia | LBA | L |
| X | 990125 | 23: 9: 7 | -12.37 | -62.14 | Brazil Rhondonia | LBA | L |
| Y | 990207 | 18:59:24 | -10.73 | -61.56 | Brazil Rhondonia | LBA | L |
| Z | 990207 | 19:19:23 | -10.71 | -61.62 | Brazil Rhondonia | LBA | L |
| a | 990210 | 18:14:13 | -10.74 | -61.92 | Brazil Rhondonia | LBA | L |
| b | 990212 | 18:14:24 | -11.33 | -61.86 | Brazil Rhondonia | LBA | L |
| c | 990212 | 20:52:23 | -10.99 | -61.22 | Brazil Rhondonia | LBA | L |
| d | 990221 | 18:42:11 | -10.58 | -60.96 | Brazil Rhondonia | LBA | L |
| e | 010820 | 21:17:20 | 18.37 | -86.46 | Trop Storm Chantal | CAMEX4 | T |
| f | 010922 | 19:36: 4 | 29.37 | -66.67 | Trop Depress Humberto | CAMEX4 | T |
| g | 010907 | 17:36:47 | 26.18 | -83.57 | Gulf of Mexico (FL) | CAMEX4 | T |
| h | 010919 | 17:58: 1 | 24.71 | -80.96 | Key West ocean | CAMEX4 | S |
| i | 010919 | 18:14:42 | 24.70 | -80.93 | Key West ocean | CAMEX4 | S |
| j | 020707 | 20:26:28 | 26.44 | -82.40 | Florida sea breaze | CRYSTAL | S |

Table 2. Convection cases. Cont'd.

| ID | DATE | TIME | LAT | LON | DESCRIPTION | CAMPAIGN | CATEG |
|---|---|---|---|---|---|---|---|
| **k** | 020707 | 21:35:20 | 25.66 | -81.29 | Florida sea breaze | CRYSTAL | S |
| **l** | 020716 | 19:45:40 | 25.67 | -80.61 | Florida land | CRYSTAL | L |
| **m** | 020723 | 20: 5:56 | 27.32 | -80.42 | Florida sea breaze | CRYSTAL | S |
| **n** | 020728 | 20:47:60 | 26.27 | -81.29 | Florida land | CRYSTAL | L |
| **o** | 020728 | 21:55:52 | 26.40 | -81.87 | Florida sea breaze | CRYSTAL | S |
| **p** | 050702 | 15: 9:11 | 15.05 | -80.96 | Caribbean Ocean | TCSP | O |
| **q** | 050707 | 0:55:37 | 16.11 | -73.20 | Hurricane Dennis Cat. 1 | TCSP | T |
| **r** | 050707 | 1:32:60 | 16.52 | -73.25 | Hurricane Dennis Cat. 1 | TCSP | T |
| **s** | 050709 | 14:29:56 | 24.55 | -83.52 | Hurricane Dennis Cat. 2 | TCSP | T |
| **t** | 050717 | 7:53:20 | 17.89 | -81.80 | Hurricane Emily Cat. 4 | TCSP | T |
| **u** | 050717 | 8:44:20 | 17.91 | -82.05 | Hurricane Emily Cat. 4 | TCSP | T |
| **v** | 050720 | 6:40: 1 | 10.59 | -86.43 | Costa Rica Pacific Ocean | TCSP | O |
| **w** | 050723 | 8:42:25 | 13.12 | -84.64 | Nicaragua land | TCSP | L |
| **x** | 050723 | 9:19:41 | 11.29 | -82.60 | Caribbean Ocean | TCSP | O |
| **y** | 050724 | 4:52: 5 | 21.15 | -94.29 | Trop Storm Gert | TCSP | T |
| **z** | 070717 | 16:15:18 | 5.60 | -82.01 | Caribbean Ocean | TC4 | O |
| **1** | 070719 | 14:23:46 | 9.10 | -85.43 | Costa Rica Pacific Ocean | TC4 | O |
| **2** | 070724 | 13:23:42 | 6.74 | -86.39 | Costa Rica Pacific Ocean | TC4 | O |
| **3** | 070724 | 13:29:46 | 6.37 | -85.85 | Costa Rica Pacific Ocean | TC4 | O |
| **4** | 070724 | 13:40:30 | 5.69 | -84.90 | Costa Rica Pacific Ocean | TC4 | O |
| **5** | 070724 | 13:29:28 | 6.38 | -85.88 | Costa Rica Pacific Ocean | TC4 | O |
| **6** | 070724 | 14:54:50 | 6.02 | -85.73 | Costa Rica Pacific Ocean | TC4 | O |
| **7** | 070724 | 15: 3:11 | 6.57 | -86.52 | Costa Rica Pacific Ocean | TC4 | O |
| **8** | 070725 | 15: 3:22 | 15.92 | -82.65 | Caribbean Ocean | TC4 | O |
| **9** | 070731 | 16: 1:59 | 9.09 | -84.80 | Costa Rica Pacific Ocean | TC4 | O |
| **#** | 070731 | 16:35:49 | 8.96 | -84.94 | Costa Rica Pacific Ocean | TC4 | O |
| ***** | 070808 | 16:17:24 | 7.92 | -83.92 | Costa Rica Pacific Ocean | TC4 | O |
| **$** | 070808 | 16:19: 8 | 7.84 | -83.76 | Costa Rica Pacific Ocean | TC4 | O |

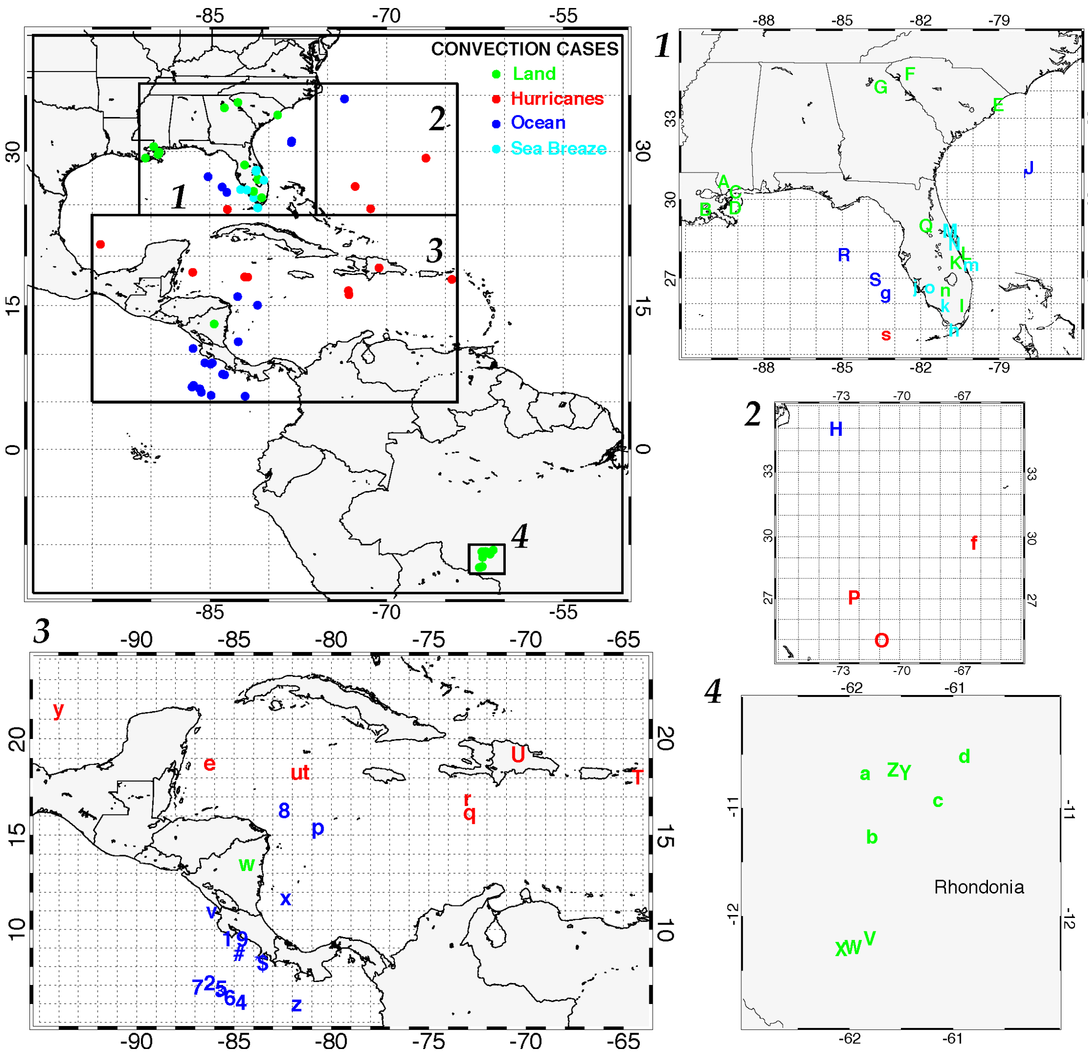


Figure 1. Map showing locations all cases from Table 2 (top left panel) along with four subset regions. Each case is denoted with a symbol provided in Table 2. The convection cases are color coded according to convection type (Land, Tropical Storms, Ocean, and Sea Breeze). Zoomed subset regions 1-4 are shown along with case locations; Rondonia is in Brazil.

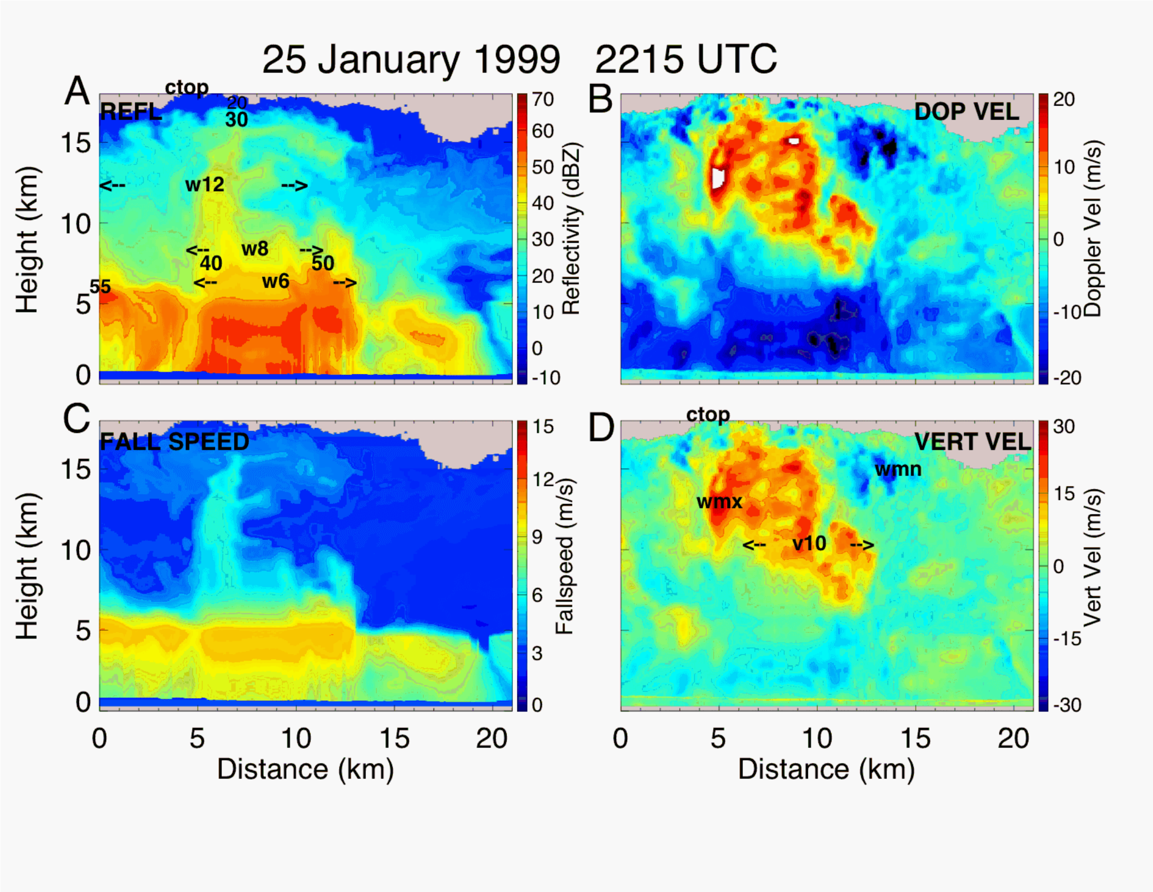


Figure 2. EDOP color cross sections for convection in Brazil Amazonia on 25 January 1999 [Case "V"]. A) reflectivity, B) Doppler velocity corrected for aircraft motions, C) fallspeed, and D) vertical velocity. Locations of quantities derived from the data are also shown on the images A and D. Panel A: heights of contour levels (20, 30, 40, 50, 55 dBZ), width of 35 dBZ at 6 km altitude (w6), width of 35 dBZ contour at 8 km altitude (w8), width of 30 dBZ contour at 12 km altitude (w12), and maximum cloud top (CTOP). Panel D: updraft maximum (WMX) and minimum (WMN), CTOP, and width of 5 $ms^{-1}$ updraft bounds at 10 km altitude. See text for details.

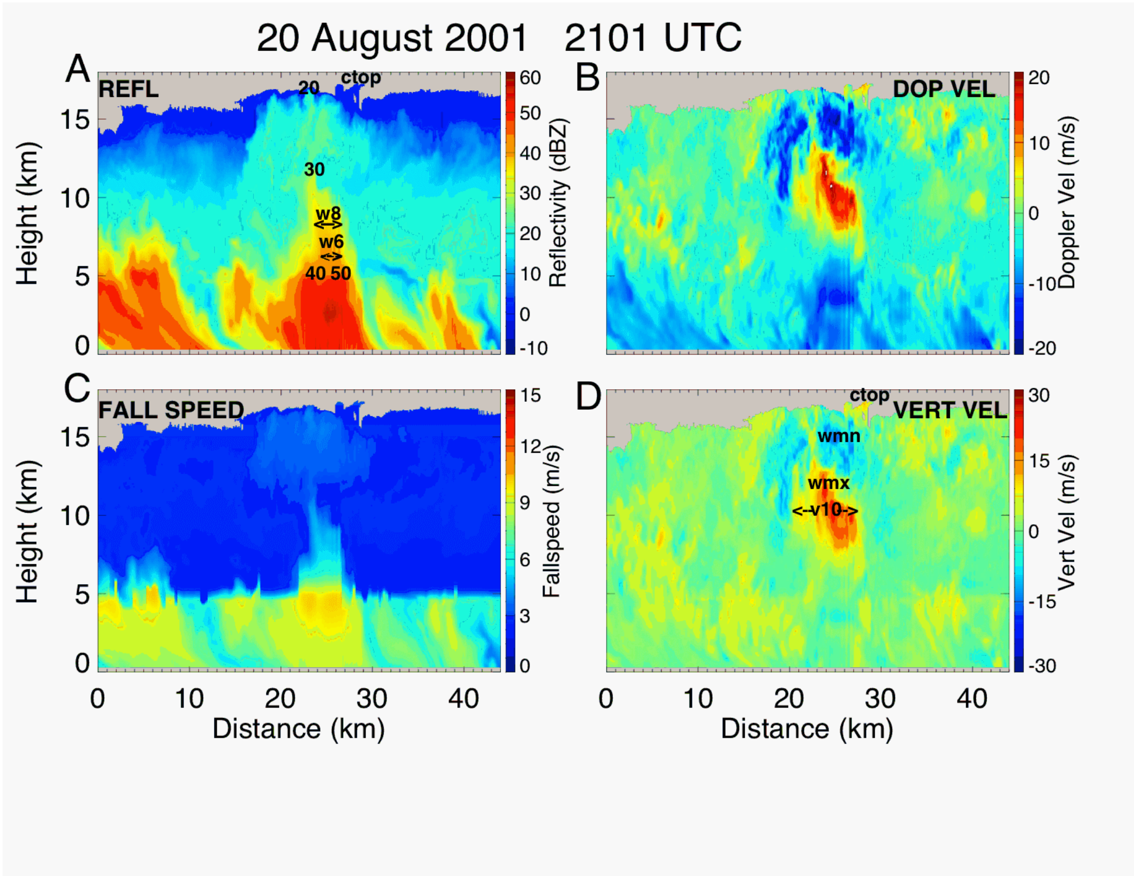


Figure 3. Similar to Fig. 2 except for the case on 20 August 2001 (Tropical Storm Chantal) [Case "e"].

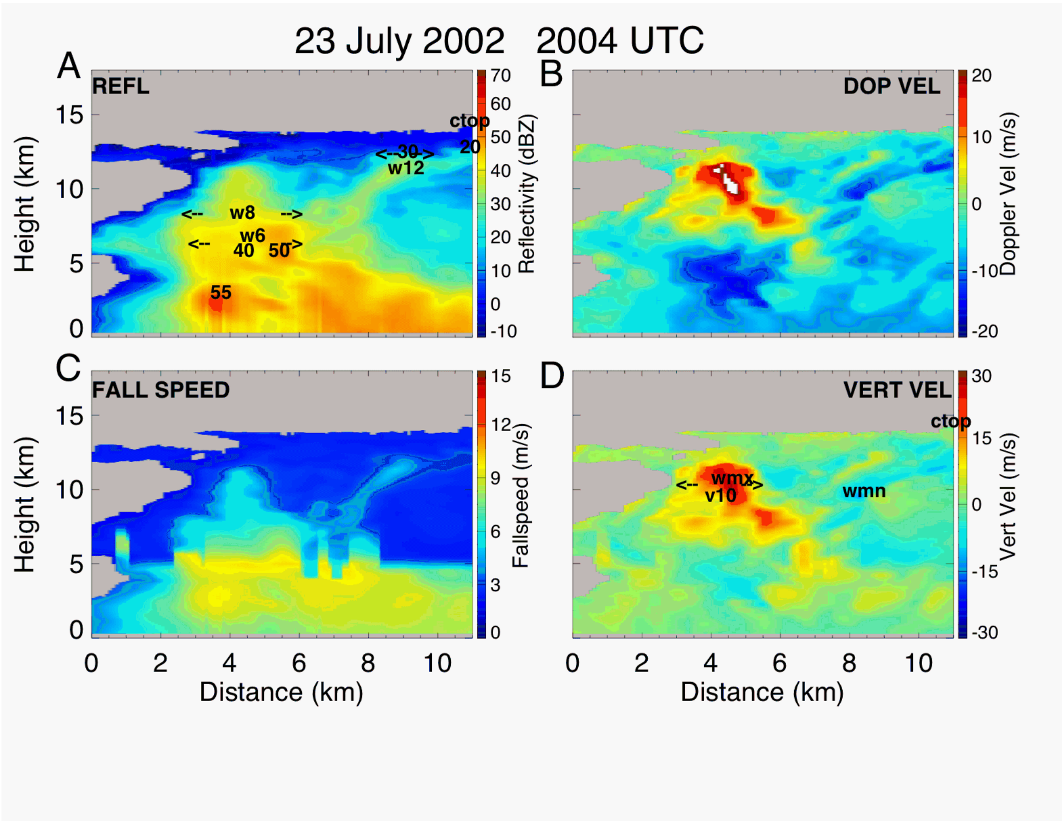


Figure 4. Similar to Fig. 2 except for the case on 23 July 2002 thunderstorm over Florida [Case “m”].

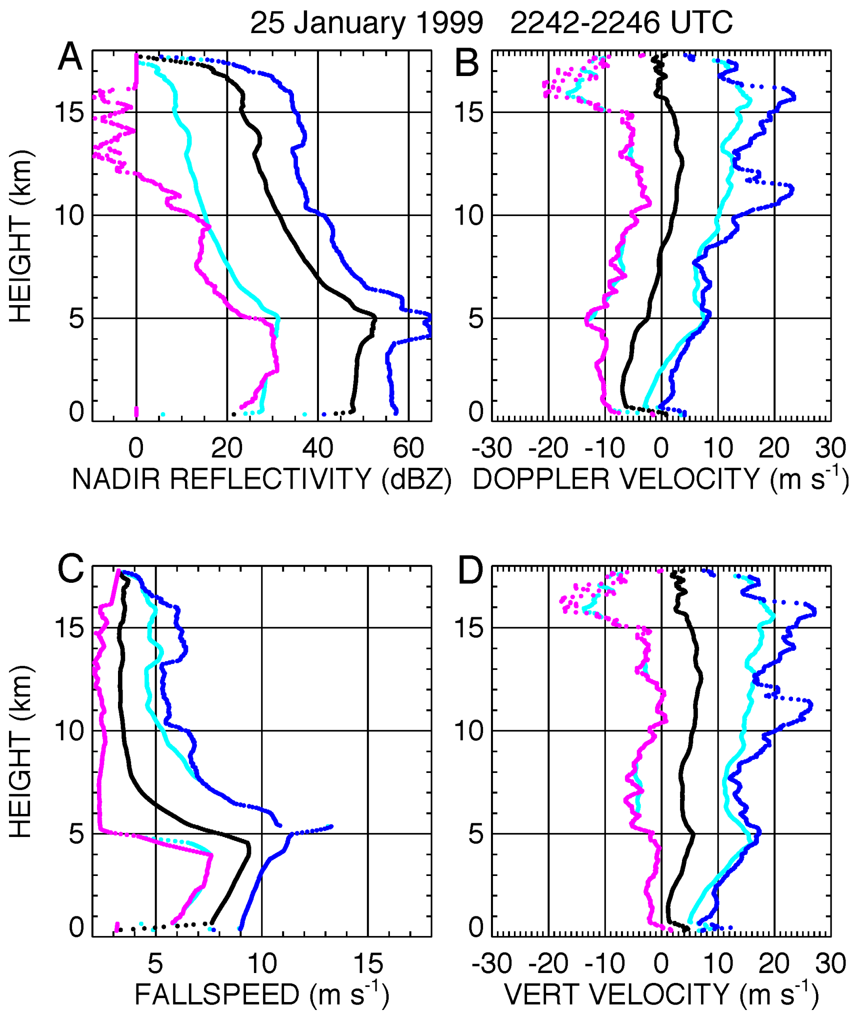


Figure 5. Profiles of nadir reflectivity (A), Doppler velocity (B), fallspeed (C), and vertical velocity (D) for 25 January 1999 corresponding to flight line in Fig. 2. The minimum (purple), maximum (blue), mean (black), and +/-2σ values (purple) are shown.

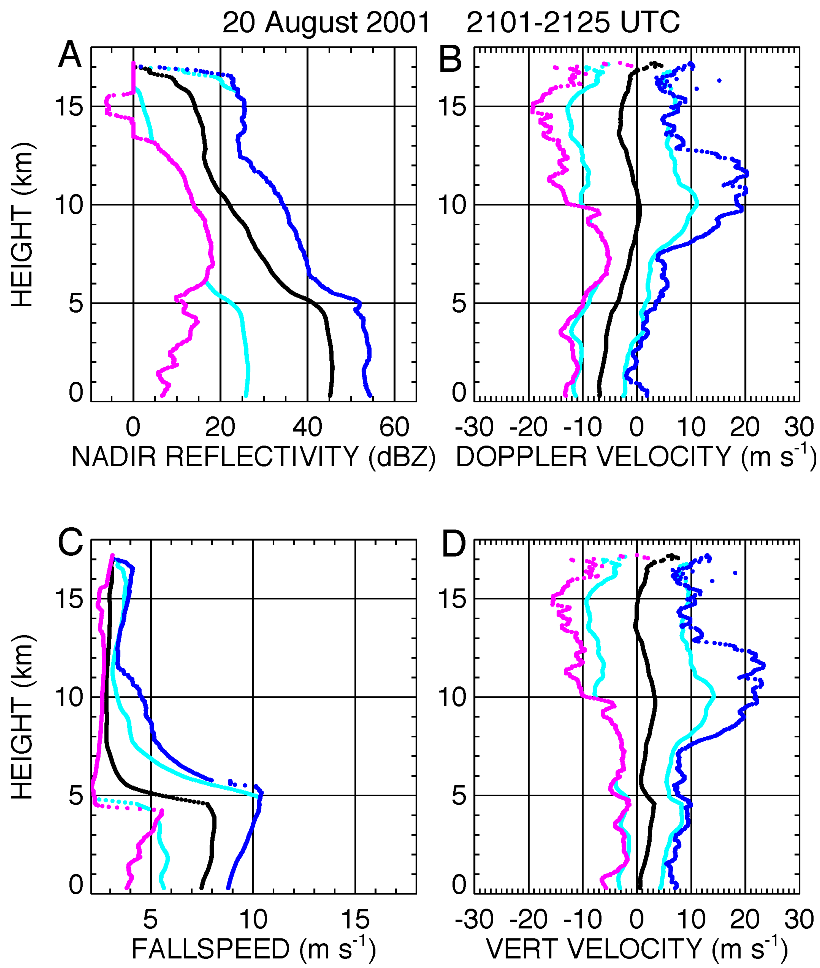


Figure 6. Same as Fig. 5 except for 20 August 2001 and corresponding to Fig. 3.

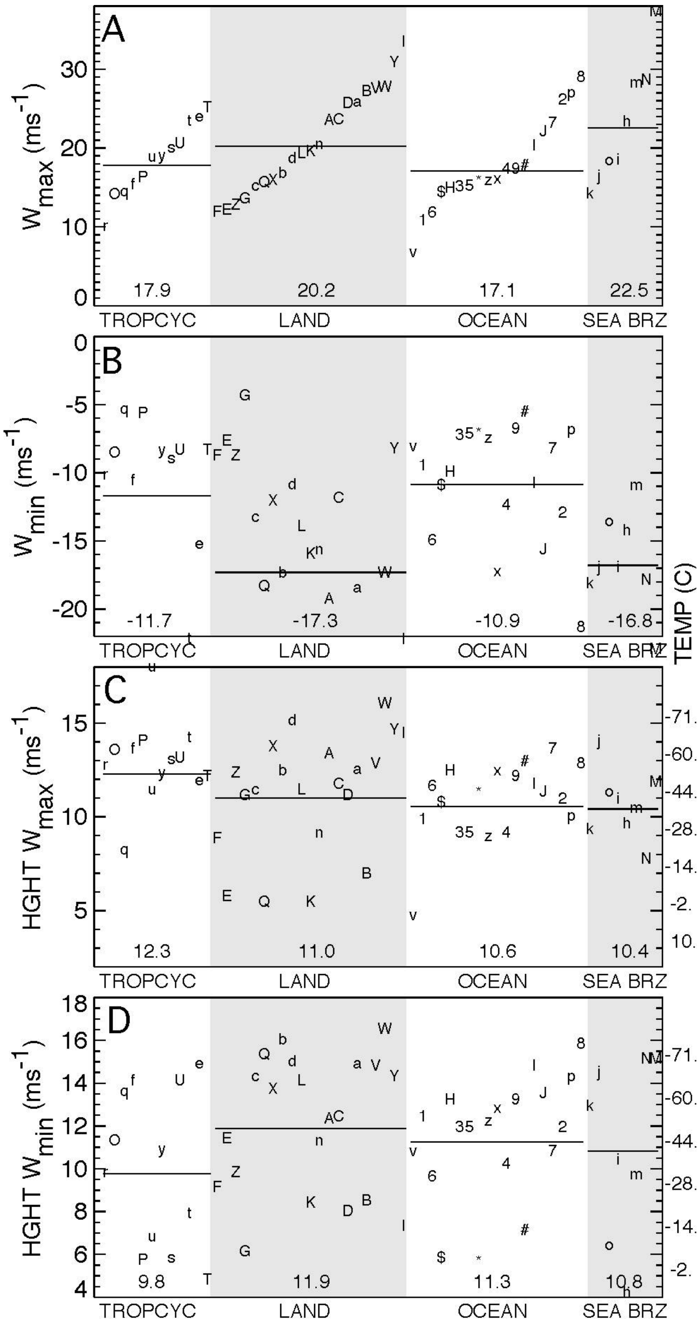


Figure 7. Updraft maxima (A) downdraft maxima (B), height of updraft maxima (C), and downdraft maxima height (D), for all cases. Characters and numbers in figure are referenced to cases in Table 1. Four categories of convection: tropical cyclone, land (shaded), oceanic, sea breeze (shaded); within each category, peak updraft increases toward the right. Shaded region highlights land-based and sea-breeze convection cases. Horizontal line provides mean for each group and actual mean is given at bottom of each group. Approximate environment temperature scale is provided on right of panels B-D.

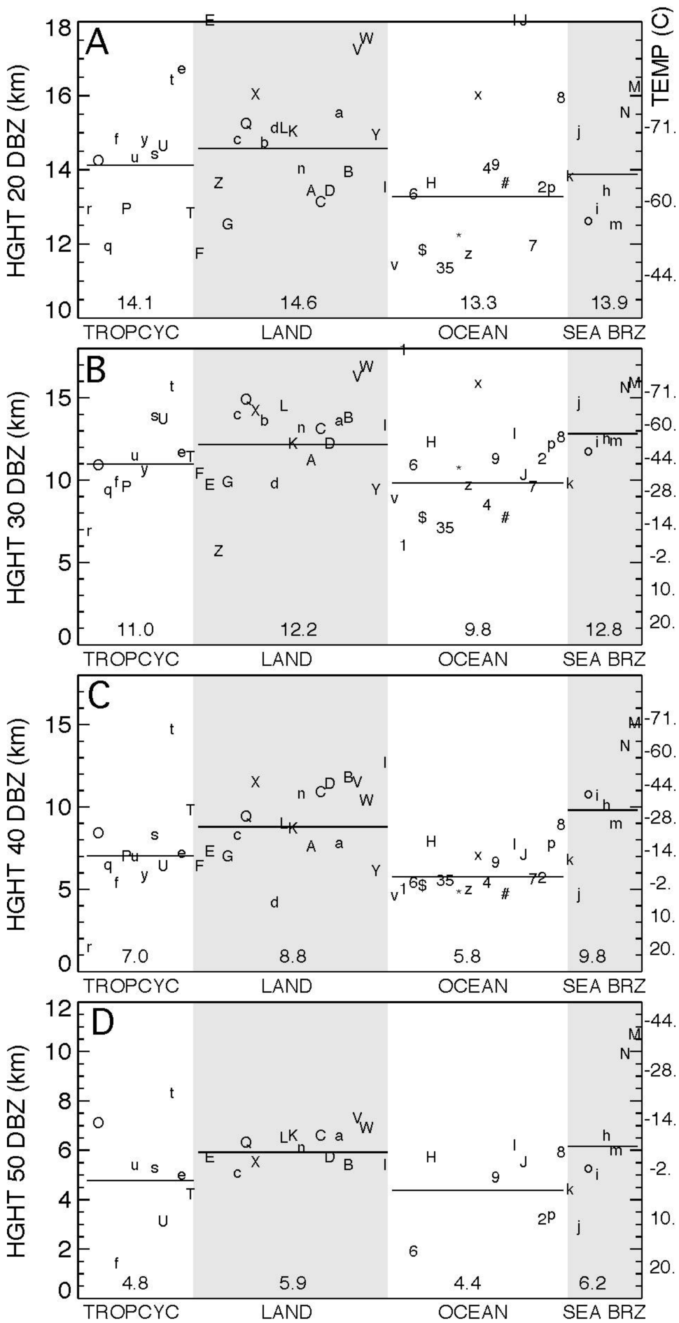


Figure 8. Maximum heights for 20 dBZ (A), 30 dBZ (B), 40 dBZ (C), and 50 dBZ (D) radar echoes. Otherwise, similar to Fig. 7.

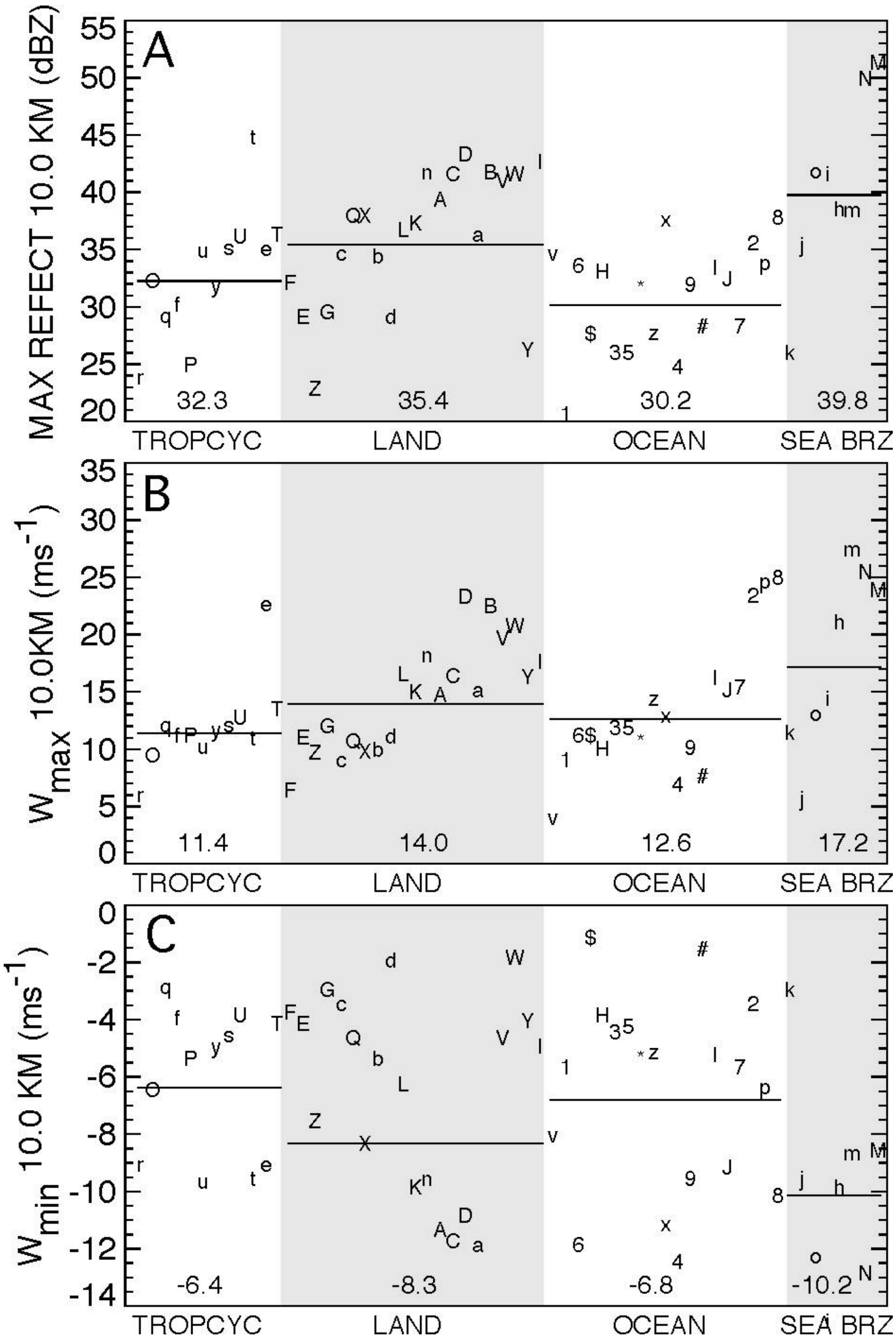

Figure 9. At 10 km level, maximum reflectivity (A), updraft maxima (B), and downdraft maxima (C), for all cases. Otherwise, similar to Fig. 7.

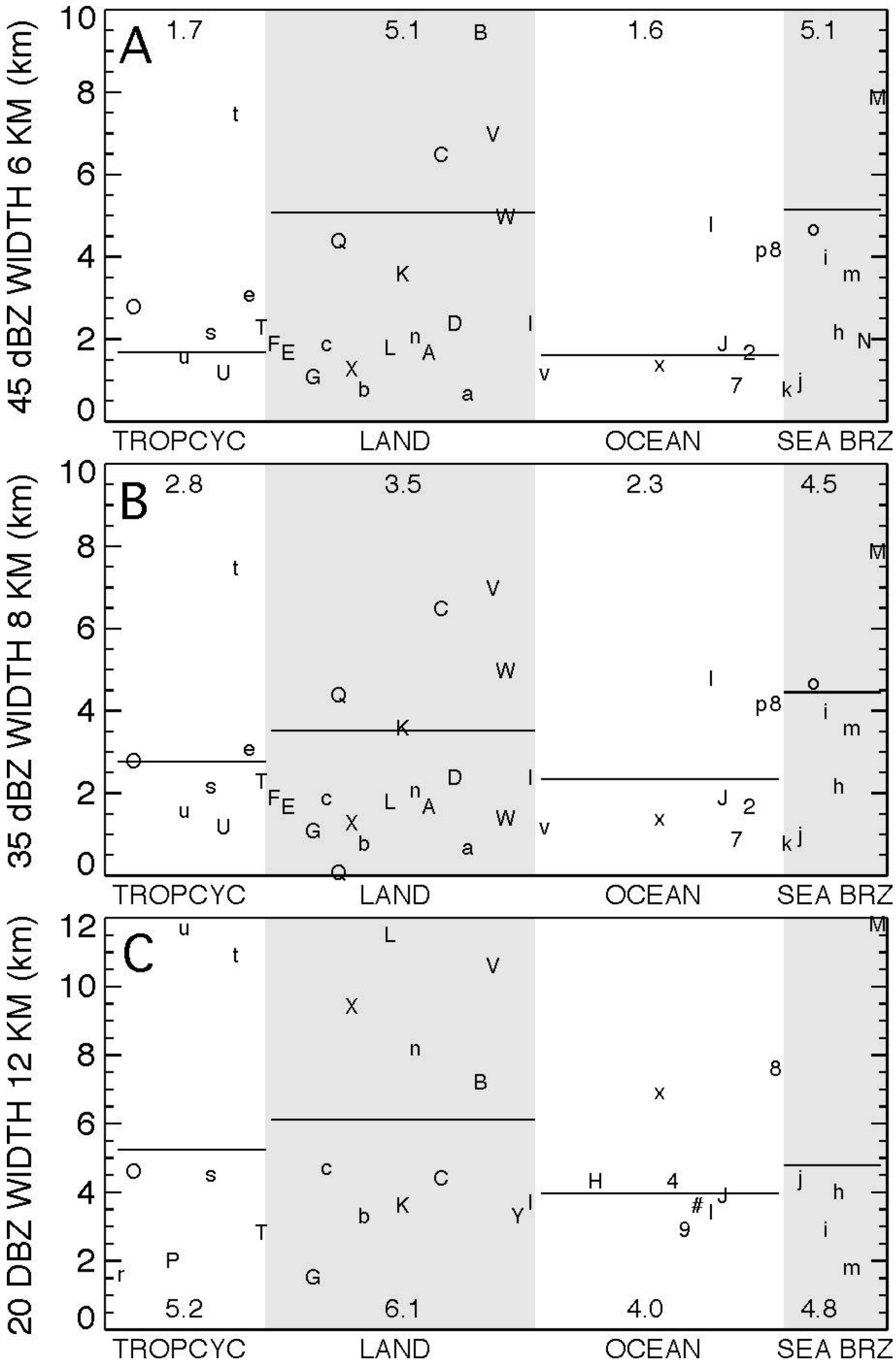


Figure 10. Widths of reflectivity cores: 45 dBZ at 6 km (A), 35 dBZ at 8 km (B), and 20 dBZ at 12 km (C). Otherwise, similar to Fig. 7.

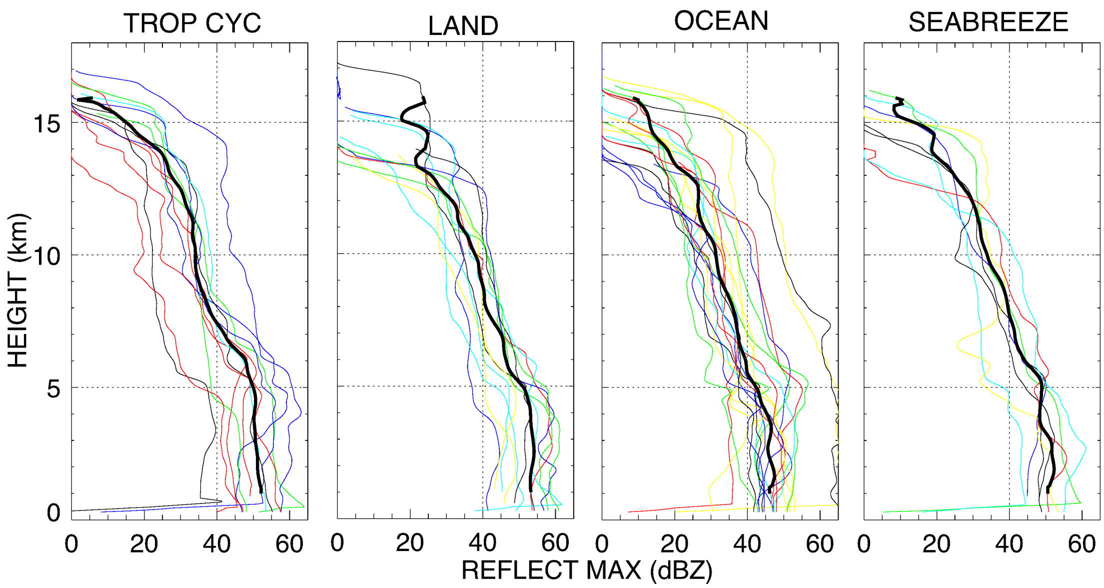


Figure 11. Comparison of maximum reflectivity profiles sorted into 4 classes of convection. Individual (non black) profiles are from each case in Table 2, black curves are mean in each class. Dotted lines are provided for reference.

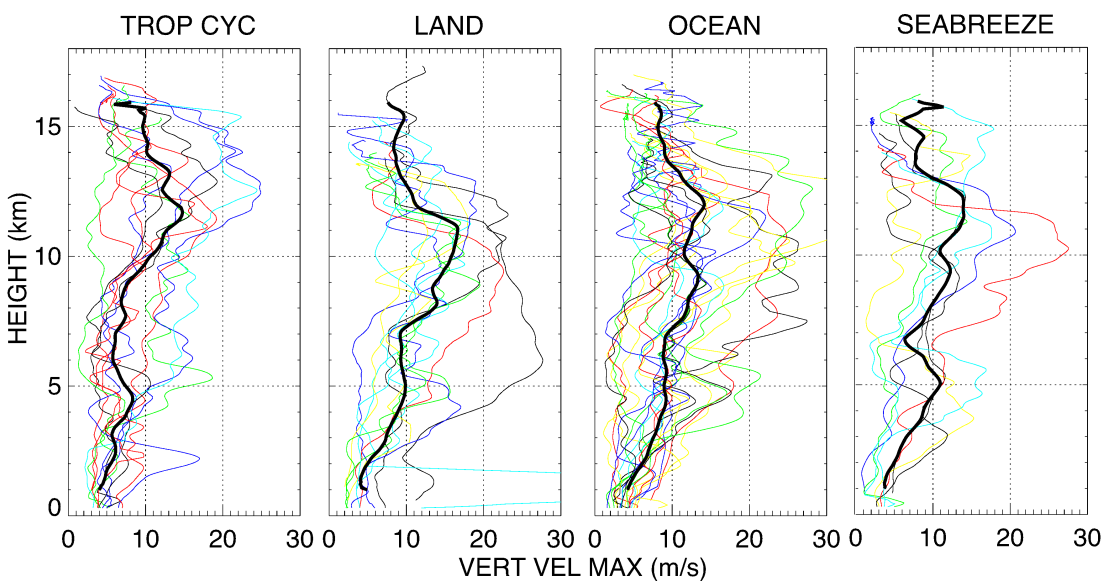


Figure 12. Similar to Fig. 11 except for peak updraft magnitudes.

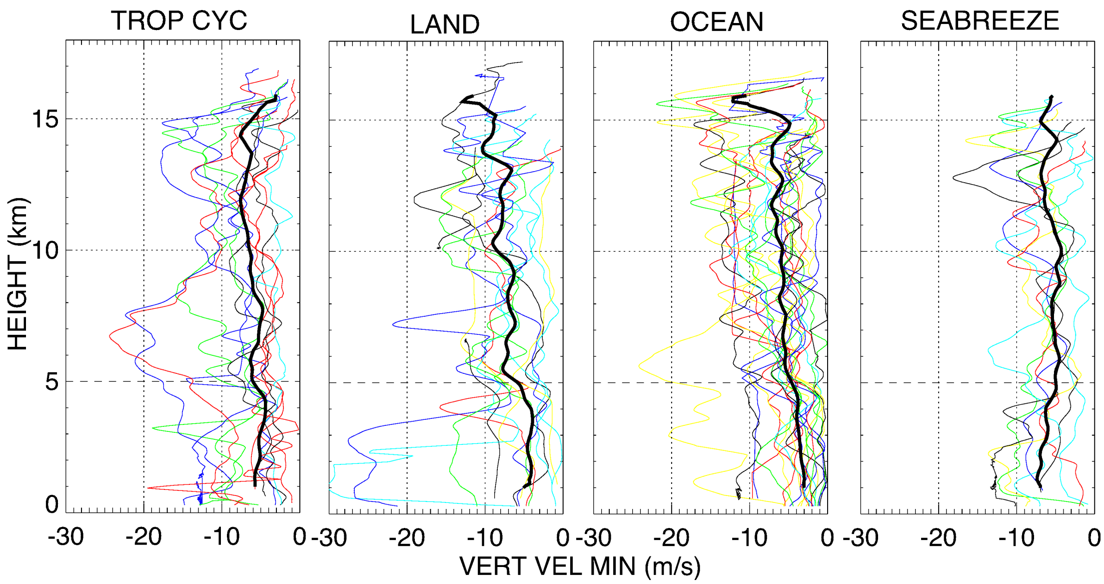

Figure 13.  Similar to Fig. 11 except for peak downdraft magnitudes.

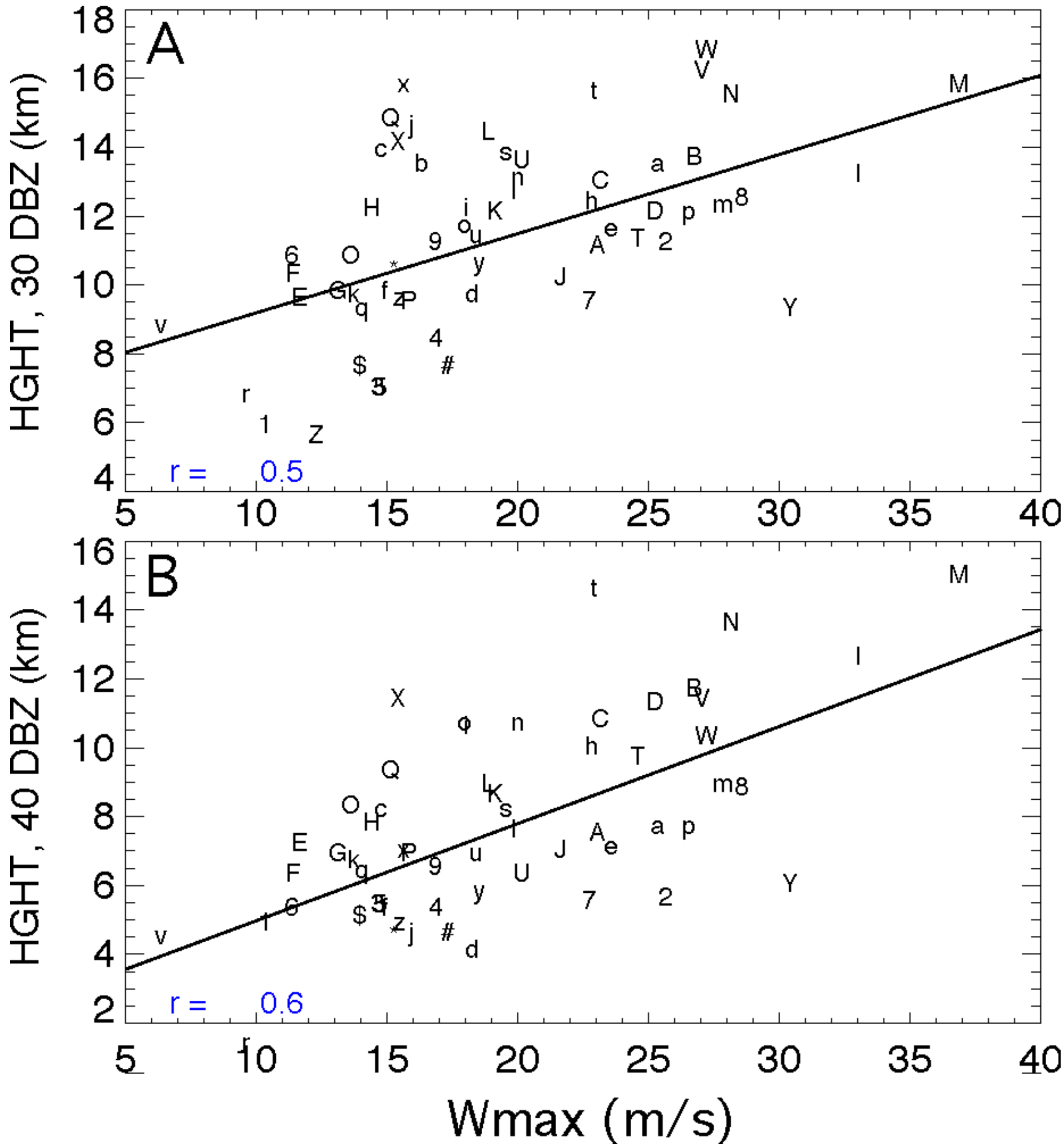


Figure 14. Relation between $w_{max}$ and maximum heights attained by 30 dBZ (A) and 40 dBZ (B) reflectivity contours. Symbols for individual cases are from Table 2. Linear fit and correlation coefficient *r* are provided in each plot.

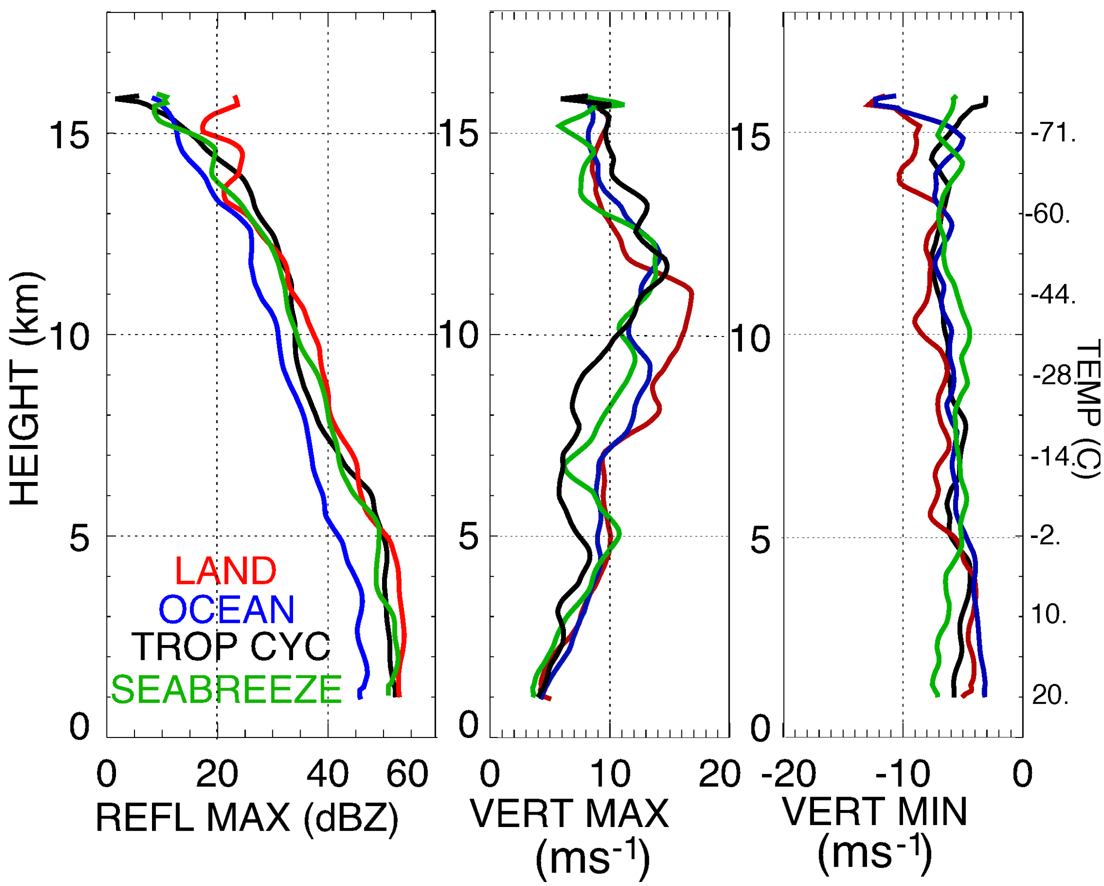


Figure 15. Mean profiles for land, ocean, tropical cyclone, and sea breeze convection types that summarize Figs 11-13. Temperature scale from Jordan mean sounding is shown on right side of figure..

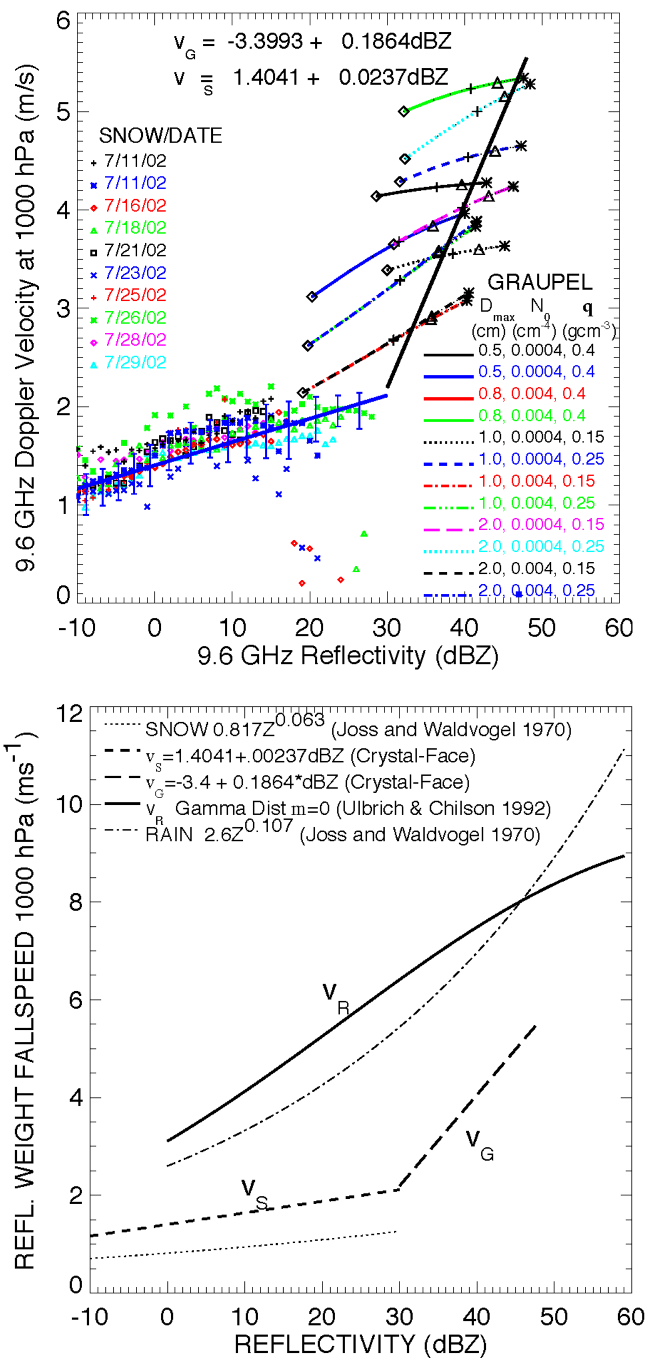


Figure A1. Fallspeed relations. Panel A provides snow fallspeeds based on in situ observations and theoretical graupel fallspeeds based on observed graupel characteristics. The symbols for snow (<30 dBZ) each represent an average of all points for a single flight in 1 dBZ intervals. IWC increases from 0.01 gm$^{-3}$ to 2 gm$^{-3}$ on the graupel curves on the right side of the plot. Linear fits (black solid curves) are given for the snow and graupel points; the graupel fit is through IWC = 1 gm$^{-3}$ points. Panel B shows fallspeed relations used in Doppler velocity-derived vertical velocities.

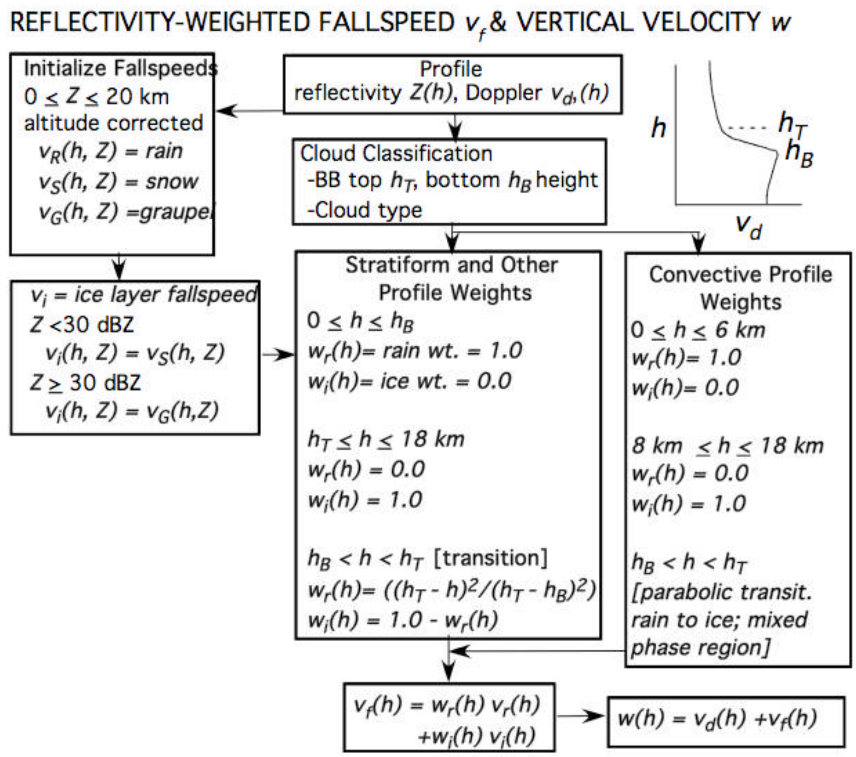


Figure A2. Fallspeed and vertical velocity calculation.